A STUDY ON WIRELESS CHANNEL MODELS: SIMULATION OF FADING, SHADOWING AND FURTHER APPLICATIONS

A Thesis Submitted to
the Graduate School of Engineering and Sciences of
İzmir Institute of Technology
in Partial Fulfillment of the Requirements for the Degree of

MASTER OF SCIENCE

in Electrical and Electronics Engineering

by
Ali ARSAL

August 2008
İZMİR

We approve the thesis of **Ali ARSAL**

Assist. Prof. Dr. Serdar ÖZEN
Supervisor

Assist. Prof. Dr. Berna ÖZBEK
Committee Member

Assist. Prof. Dr. Olcay AKAY
Committee Member

28 AUGUST 2008
Date

Prof. Dr. F. Acar SAVACI
Head of the Department of Electrical and Electronics Engineering

Prof. Dr. Hasan BÖKE
Dean of the Graduate School of Engineering and Science

ACKNOWLEDGEMENTS

I would like to express my sincere gratitude to my advisor Dr. Serdar Özen, for his help, guidance, understanding and encouragement during the study and preparation of this thesis.

I would like to thank to the members of my Thesis Committee, Dr. Berna Özbek and Dr. Olcay Akay for their useful comments. I also would like to thank to Kadir Atilla Toker, whom I had the pleasure of working with.

This thesis has been supported by EU-FP6 ”Marie Curie” International Reintegration Grant, Contract No: 029157.

Finally, I thank my parents who always supports me throughout my whole education life.

ABSTRACT

A STUDY ON WIRELESS CHANNEL MODELS: SIMULATION OF FADING, SHADOWING AND FURTHER APPLICATIONS

In this thesis, we simulate multipath fading which is assumed to have Rayleigh or Rician distribution under the non-line-of sight or line-of-sight condition respectively; as well as spatial shadowing process, assumed to be log-normally distributed. We propose a low-complexity high performance Rayleigh fading simulator, an autoregressive moving average (ARMA)(3,3) model. This proposed method is a variant of the method of filtering of the white Gaussian noise where the filter design is accomplished in the analog domain and transferred into the digital domain. The proposed model is compared with improved Jakes' model, autoregressive (AR) filtering and inverse discrete Fourier transform (IDFT) techniques, in performance and computational complexity. The proposed method outperforms AR(20) filter and modified Jakes' generators in performance. Although IDFT method achieves the best performance, it brings a significant cost in storage which is undesirable. The proposed method achieves high performance with the lowest complexity. Additionally, we apply the quantized filter extension of our proposed filter design, since quantized filters are generally used in hardware implementations due to their minimum power consumption, minimum heat generation and their computational efficiency. We simulate spatial shadowing process, via the simulation method proposed by Pätzold and Nguyen. This method is derived from a reference model by using the sum of sinusoids principle. There are two methods enabling the fitting of the simulation model to the reference model with respect to the probability density function (pdf) of the received signal strength as well as to a given autocorrelation function with a decaying exponential shape. Furthermore we use our predicted autocorrelation function obtained via the site-specific radio propagation prediction software named Wireless InSite in order to determine the model parameters.

ÖZET

KABLOSUZ KANAL MODELLERİ ÜZERİNE BİR ÇALIŞMA: SÖNÜMLEMENİN, GÖLGELEMENİN VE DAHA İLERİ UYGULAMALARIN BENZETİMİ

Bu tezde, doğrudan görüş bulunmayan durumlarda ve doğrudan görüş bulunan durumlarda, sırasıyla Rayleigh ya da Rician dağılıma sahip çok yollu sönümlemenin, log-normal dağılıma sahip olduğu varsayılan uzamsal gölgeleme süreciyle birlikte benzetimini yaptık. Düşük karmaşıklığa ve yüksek performansa sahip bir Rayleigh sönümleme benzeticisi, özbağlanımlı hareketli ortalama (ARMA)(3,3) modeli sunduk. Sunulan bu yöntem bir çeşit beyaz Gauss gürültüsü süzgeçleme yöntemidir. Burada süzgeç tasarımı analog bölgede yapılır ve sayısal bölgeye transfer edilir. Sunduğumuz yöntemi, iyileştirilmiş Jakes modeliyle, özbağlanımlı (AR) süzgeçlemeyle ve ters ayrık Fourier dönüşümü (IDFT) teknikleriyle performans ve işlemsel karmaşıklık açısından karşılaştırdık. Sunduğumuz yöntem, AR(20) süzgecinden ve iyileştirilmiş Jakes modelinden daha iyi performans sağladı. IDFT yöntemi en iyi performansı sağlamasına rağmen depolama açısından belirgin bir yük getirdi. Sunduğumuz yöntem en iyi performansı en düşük karmaşıklıkla sağladı. Nicemlenmiş süzgeçler genellikle, düşük güç tüketiminden, düşük ısı üretiminden ve işlemsel etkinliğinden dolayı donanım uygulamalarında kullanılmaktadır. Bu yüzden, sunduğumuz yöntemin nicemlenmiş süzgeç uygulamasını da yaptık. Uzamsal gölgeleme sürecinin benzetimini ise Pätzold ve Nguyen tarafından sunulan benzetim yöntemiyle yaptık. Bu yöntem referans modelden sinuzoidlerin toplamı prensibi kullanılarak çıkarılmıştır. Benzetim modelini referans modele uydurmak için, kullanılan iki yöntem vardır. Bu yöntemler alınan sinyalin olasılık yoğunluk fonksiyonuyla birlikte teorik öz ilinti fonksiyonuna göre belirlenir. Biz bu yaptıklarımıza ek olarak, ayrıca Wireless InSite yazılımıyla kestirdiğimiz öz ilinti fonksiyonunu kullanarak model parametrelerini belirledik.

TABLE OF CONTENTS

LIST OF FIGURES

LIST OF TABLES

Table **Page**

CHAPTER 1

INTRODUCTION

1.1. Background and Motivation

The performance of any communication system is eventually determined by the medium which the message signal passes through. This medium, may be an optical fiber, a hard disk drive of a computer or a wireless link, is referred to as communication channel. There exists a large variety of channels, which may be divided into two groups. If a solid connection exists between transmitter and receiver, the channel is called a wired channel. If this solid connection is missing, this connection is called a wireless channel. Wireless channels differ from wired channels, due to their unreliable behavior compared to wired channels. In wireless channels the state of the channel may change within a very short time span. This random and severe behavior of wireless channels turns communication over such channels into a difficult task.

There are several different classifications regarding the wireless channels. Wireless channels may be distinguished by the propagation environment encountered. Many different propagation environments have been identified, such as urban, suburban, indoor, underwater or orbital propagation environments, which differ in various ways.

The wireless channel puts fundamental limitations on the performance of wireless communication systems. The transmission path between the receiver and the transmitter can be altered from simple line-of-sight to one that is drastically obstructed by buildings, foliage and mountains. Even the speed of the mobile impacts how rapidly the signal level fades. Modeling the wireless channel has historically been one of the most difficult parts of the communication system design and is typically done in a statistical manner, based on measurements made specifically for a designated communication system or spectrum allocation.

There are a lot of mechanisms behind the electromagnetic wave propagation, but they can be generally attributed to reflection, diffraction and scattering as shown in Figure 1.1. Reflections arise when the plane waves are incident upon a surface with dimensions that are very large compared to the wavelength. Diffraction occurs according to

Huygen's principle when there is an obstruction between the transmitter and the receiver antennas and as a result of this, there are secondary waves generated behind the obstructing body. Scattering arises when the incident wavelength is in the order of or larger than the dimension of the blocking object with non-regular shape, and causes the transmitting energy to be redirected in many directions. The relative importance of these three propagation mechanisms depends on the particular propagation scenario.

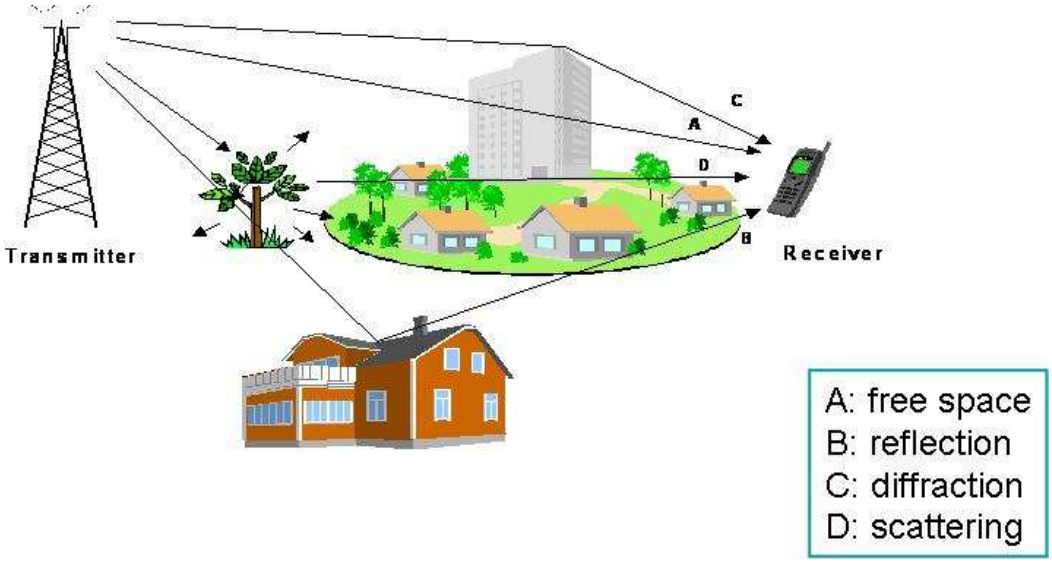

Figure 1.1. Mechanisms behind the electromagnetic wave propagation

Due to the three aforementioned different propagation mechanisms, radio propagation can be roughly described by three nearly independent phenomenon; *path loss* variation with distance, *shadowing* and *multipath fading*. Each of these phenomenon is caused by a different underlying physical principle and must be considered when designing and evaluating the performance of a wireless communication system.

Among three independent phenomenon, only path loss is a deterministic effect which depends only on the distance between the transmitter and the receiver. It plays an important role on larger time scales like seconds or minutes, since the distance between the transmitter and the receiver in most situations does not change significantly on smaller time scales. On the other hand, shadowing and fading are not deterministic. They both have stochastic nature. Shadowing occurs due to the varying terrain conditions in suburban area and due to the obstacles such as buildings etc. in urban area causing particular obstructions between the base station and mobile station. Fading leads to significant attenuation changes within smaller time scales such as milliseconds or even microsec-

onds. Fading is always caused by a multipath propagation environment, therefore by an environment reflecting the transmitted electromagnetic waves such that multiple copies of this wave interfere at the receiving antenna. All three attenuating phenomenon combined result in the actual experienced attenuation of the wireless channel. Therefore this attenuation might be decomposed as given in Equation (1.1).

$$a(t) = a_{PL}(t) \cdot a_{SH}(t) \cdot a_{FA}(t) \tag{1.1}$$

In this thesis we will focus on modeling and simulation of fading and also modeling and analysis of shadowing. We will investigate a new simulator design for multipath fading and also we will model and analyze the correlations that exist in shadowing.

The fading caused by multipath propagation in wireless communication systems is commonly modeled by the Rayleigh distribution. It is well known that a Rayleigh fading process is characterized by its power spectral density and its auto-correlation function. The autocorrelation function depends on the Doppler frequency which corresponds to the relative motion of the receiver and transmitter.

In the communications literature, a number of different methods have been proposed and used for the simulation of Rayleigh fading (Clarke 1968, Jakes 1974, Smith 1975, Pätzold, et al. 1996, Omidi, et al. 1999, Young and Beaulieu 2000, Özen and Zoltowski 2001, Zheng and Xiao 2002, Baddour and Beaulieu 2005). Jakes' model (Jakes 1974) has been of great interest which is based on sum of sinusoids approach. Simulators based on white noise filtering methods (Omidi, et al. 1999, Özen and Zoltowski 2001, Baddour and Beaulieu 2005), and on the Inverse Discrete Fourier Transform (IDFT) (Smith 1975, Young and Beaulieu 2000) method have also become popular. It was shown in (Young and Beaulieu 2001) that the fading signals which are produced by classical Jakes' simulator are not wide-sense stationary (WSS). On the other hand simulators based on the IDFT method are high-quality and efficient. Unfortunately, a disadvantage of the IDFT method is that all samples are generated with a single fast Fourier transform (FFT), hence the storage requirements make it useless for the generation of very large number of samples and for sample-by-sample simulations.

In this thesis, we consider using a fading filter to filter white Gaussian noise that was first proposed in (Özen and Zoltowski 2001). Unlike the other filter structures (Omidi, et al. 1999, Baddour and Beaulieu 2005), a different optimization and de-

sign criterion is used to set the filter parameters in the analog domain as would yield the transfer function of the fading filter, denoted by $G_\gamma(s)$, where γ is the filter order. Bilinear transform is then used to get the desired filter structure as an ARMA(γ, γ) filter. Comparisons to other methods are then made by using quantitative measures introduced in (Young and Beaulieu 2003).

Experimental results have shown that the signal strength variations caused by shadowing can adequately be modeled by a log-normal process (Okumura, et al. 1968, Reudink 1972, Black and Reudink 1972, Ibrahim and Parsons 1983, Gudmundson 1991). Measurements also show that the shadowing exhibits spatial correlation (Gudmundson 1991, Marsan and Hess 1990, Giancristofaro 1996, Perahia and Cox 2001) in other words, shadowing is correlated over short distances. A simple exponential correlation model has been suggested in (Gudmundson 1991), based upon an approximate fitting of empirical data. This model was improved then later in (Giancristofaro 1996) to avoid the inconsistencies caused by the exponential shape of the spatial autocorrelation function. In this thesis, we simulate spatial shadowing process via the simulation model proposed in (Pätzold and Nguyen 2004). Also, we predict an autocorrelation function and this function is used to determine the model parameters.

1.2. Outline

After the introduction, which contains a brief summary of some useful terms that will be used in this thesis, a detailed overview of *fading* phenomenon is provided in Chapter 2. In Chapter 3, different simulation techniques commonly employed to simulate fading channels are discussed. The first part of Chapter 3 concerns with the sum of sinusoids models and in the second part, different kind of filtered Gaussian noise models including our proposed filter design are discussed. Also in Chapter 3, quantized filter application of our proposed design is given. In Chapter 4, large-scale fading study is undertaken with shadowing prediction experiment made by Wireless InSite. In Chapter 5, simulation of spatial shadowing process is done by using the simulation model proposed in (Pätzold and Nguyen 2004). Also in this chapter, prediction of shadowing autocorrelation in an urban area is made by using Wireless InSite. We use this autocorrelation in order to determine the simulation model parameters of the spatial shadowing process. The last chapter is entirely dedicated to the discussion and interpretation of the presented results.

CHAPTER 2

AN OVERVIEW OF WIRELESS CHANNEL MODELS

2.1. Introduction

In digital communication theory the most frequently assumed model for a transmission channel is the additive white Gaussian noise (AWGN) channel. However, for many communication systems the AWGN channel is a poor model, hence the need to resort to more precise and complicated channel models. One basic type of non-Gaussian channel, which frequently occurs in practice, is the fading channel. A typical example of such a fading channel is the mobile radio channel, where the small antennas of portable units pick up several multipath reflections. As a result, the mobile channel exhibits a time varying behavior in the received signal energy, which is called fading. In the communications literature, most often we encounter two types of fading definitions for the mobile radio channel, and they are called *large-scale fading* and *small scale fading*. Large-scale fading usually is defined as the average signal power attenuation or path loss due to motion over large areas. This depends on the presence of obstacles in the signal path, on the position of the mobile unit and its distance from the transmitter. The statistics of large-scale fading provide a way of computing an estimate of path loss as a function of distance. This is normally described in terms of a mean-path loss (nth-power law) and a log-normally distributed variation about the mean which is known as shadowing. Hence the term large-scale fading correspond to the combined effects of path-loss and shadowing loss that we have indicated in Chapter one in Equation 1.1, where the path loss has been denoted by $a_{PL}(t)$ and the shadowing process has been denoted by $a_{SH}(t)$. The emphasis of this chapter and the following chapter is on the small-scale fading. The large scale fading study, also known as *shadowing and path-loss* has been undertaken in Chapters 4 and 5.

Small-scale fading refers to dramatic changes in signal amplitude and phase that can be experienced as a result of small changes in the spatial separation between a receiver and transmitter. Small-scale fading is referred to as Rayleigh fading if the multiple reflective paths are large in number and there is no line of sight signal component, hence

the envelope of the received signal is statistically described by a Rayleigh probability density function (pdf). However, if there is a dominant non-fading signal component present, such as a line-of sight propagation path, the small scale fading envelope is described by a Rician pdf. A number of different models have been proposed for the simulation of Rayleigh fading channels in the past years. Generally, these models can be classified as either being statistical or deterministic. The statistical models are based on the shaping of the power spectral densities of white Gaussian random processes by either time-domain or frequency-domain filtering, whereas the deterministic models approximate the Gaussian processes by the superposition of finite properly selected sinusoids. Details of these are presented herein.

2.2. Small Scale Fading

In a wireless mobile communication system, a signal can travel from transmitter to receiver over multiple reflective paths. The effect can cause fluctuations in the received signals amplitude, phase, and angle of arrival, giving rise to the terminology multipath fading. These signal variations are experienced on a small time scale, mostly a fraction of a second or shorter, depending on the velocity of the receiver. In this section we will discuss the physical reasons of fading, present a mathematical model for fading and characterize it as a stochastic process. Fading might have a time varying or frequency varying attenuating impact on the transmitted signal. Due to the frequency varying and time varying (complex valued) nature of fading, we will denote the attenuating impact in this Section by $\overline{H}(t, f)$. The relationship to the notation used in Equation 1.1 is given by $a_{FA}(t) = |\overline{H}(t, f)|$ for the observed carrier frequency. In some cases the fading might be only time varying or frequency varying, we denote the fading by $\overline{h}(t) = \overline{H}(t, 0)$ in the case of time varying fading only, and by $\overline{H}(f) = \overline{H}(0, f)$ in the case of frequency varying fading only.The relationship to the notation used in Equation 1.1 is in these cases still given by $a_{FA}(t) = |\overline{H}(t, f)|$ for the observed carrier frequency. The subjects discussed in this section is following the chapter about fading in (Cavers 2000).

2.2.1. Physical Basis

The physical basis of fading is given by the reception of multiple copies of the transmitted signal, each having followed a different path. Depending on the environment of transmitter and receiver, there can be many or only few objects reflecting the transmitted radio signal. In general these objects are known as *scatterers* and the transmission of a signal leads to a situation which is called a *multipath signal propagation* and an example of this scenario is given in Figure 2.1.

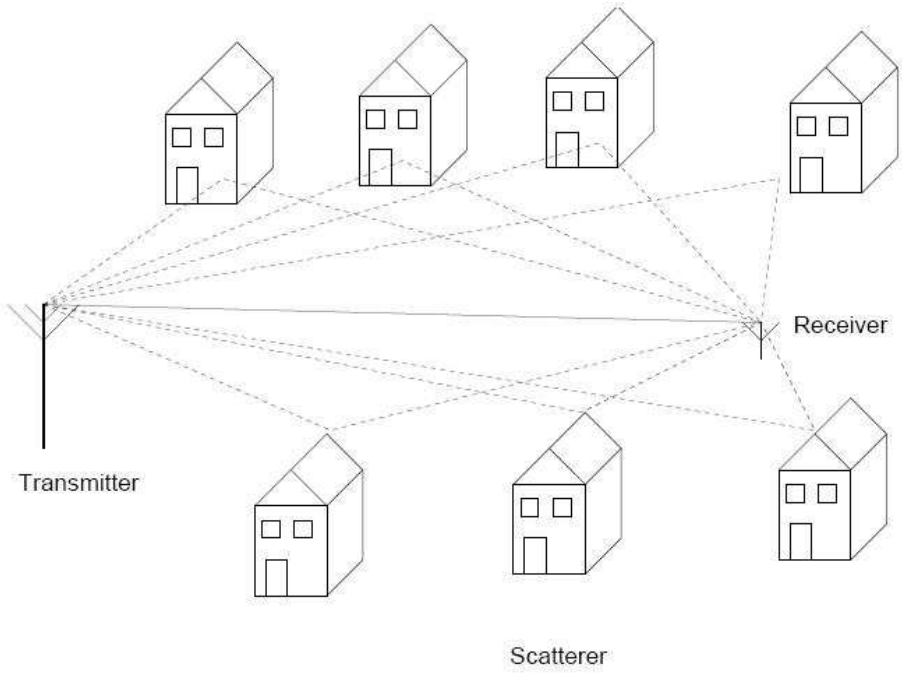

Figure 2.1. Multipath propagation scenario

In a typical environment each path *i* has a different length l_i. Because of this difference in length, each signal travelling along a path arrives with a different *delay* $\tau_i = \frac{l_i}{c}$, where c is the speed of the light. Some signal copies travelling along short paths will arrive quite fast, while other copies travelling along longer paths will arrive later. Physically this equals an echo, encountered in a canyon. The channel is said to have memory, since it is able to store signal copies for a certain time span.

Beside this multipath propagation, each signal copy is attenuated differently, since the signal paths have to pass different obstacles like windows, building walls of different materials, trees of different sizes and so on. The attenuation factor of path *i* is denoted by a_i.

Taking all this into account, the multipath propagation of a transmitted radio wave results in an interference pattern, where at certain points the wave interfere constructively while at other points they interfere destructively. If each element within the propagation environment (transmitter, scatterer, receiver) do not move, the receiving signal will only suffer from the *delay spread* and the different attenuation. In this case, the interference situation of the channel stays constant and therefore the channel is said to be time invariant. In contrast, if any kind of movement is encountered in the propagation environment, all paths or some paths change in time, such that all a_i and τ_i change in time. As a consequence the wireless channel become time variant. Here, along with a constant changing delay spread, the receiver also experiences a varying signal strength due to its movement through the interference pattern, therefore the received signal fades.

2.2.2. Mathematical Model of Fading

Consider the transmission of a bandpass signal at carrier frequency f_c with complex envelope $\overline{s}(t)$. This transmitted bandpass signal is given by Equation 2.1

$$s(t) = Re\left(\overline{s}(t) \cdot e^{2\pi j \cdot f_c t}\right) \tag{2.1}$$

The received bandpass signal is given by Equation 2.2

$$r(t) = Re\left(\overline{r}(t) \cdot e^{2\pi j \cdot f_c t}\right) \tag{2.2}$$

We look for a mathematical model of the received bandpass signal taking into account the effect of multipath propagation. At first we consider the case where we do not encounter motion in the environment. As described in previous section, each path is associated with a different length l_i and a different attenuation a_i. Therefore the received signal $r(t)$ is the superposition of all copies, given in Equation 2.3

$$r(t) = \sum_i a_i \cdot s\left(t - \frac{l_i}{c}\right) = Re\left(\sum_i a_i \cdot \overline{s}\left(t - \frac{l_i}{c}\right) \cdot e^{2\pi j \cdot f_c\left(t - \frac{l_i}{c}\right)}\right) \tag{2.3}$$

Considering the relationship between wavelength and frequency $\lambda = \frac{c}{f_c}$, we obtain a complex envelope representation in Equation 2.4. If we denote the phase shift of the carrier frequency caused by the different length of each path by $\varphi_i = 2\pi \frac{f_c l_i}{c} = 2\pi \frac{l_i}{\lambda}$ and path delay by $\tau_i = \dfrac{l_i}{c}$ we have Equation 2.4.

$$\overline{r}(t) = \sum_i a_i \cdot e^{-j2\pi \frac{l_i}{\lambda}} \cdot \overline{s}\left(t - \frac{l_i}{c}\right) = \sum_i a_i \cdot e^{-j\varphi_i} \cdot \overline{s}(t - \tau_i) \tag{2.4}$$

Now let us consider the effect of the motion in this model. The change of the path length ,as a function of speed v and time t, is given by $\Delta l_i = -v\cos(\gamma_i)t$, where γ_i denotes the angle of arrival of path i with respect to the direction of motion of the receiver. From this we obtain a different function for the complex envelope, which depends now on the time t, as given in Equation 2.5.

$$\begin{aligned}\overline{r}(t) &= \sum_i a_i \cdot e^{-j2\pi\frac{l_i+\Delta l_i}{\lambda}} \cdot \overline{s}\left(t - \frac{l_i + \Delta l_i}{c}\right) \\ &= \sum_i a_i \cdot e^{-j\varphi_i} \cdot e^{-j2\pi\cdot\cos(\gamma_i)\cdot t\frac{v}{\lambda}} \cdot \overline{s}\left(t - \tau_i + \frac{v\cdot\cos(\gamma_i)\cdot t}{c}\right) \end{aligned} \tag{2.5}$$

We can simplify Equation 2.5. First we indicate the term $a_i \cdot e^{-j\varphi_i}$ by writing $\overline{A}_i$ instead. Second if we compare the delay caused by the term $v\cdot\cos(\gamma_i)t/c$ with the overall signal length of the complex envelope $\overline{s}(t)$, this delay is so short that can be ignored. Another simplification is done through introducing the *Doppler frequency* denoted by $f_d = \frac{f_c}{c}\cdot v = \frac{v}{\lambda}$ and the *Doppler shift* denoted by $\nu_i = \cos(\gamma_i)\cdot f_d$. By doing these simplifications we obtain Equation 2.6.

$$\overline{r}(t) = \sum_i \overline{A}_i \cdot e^{j2\pi\cdot\cos(\gamma_i)\cdot t\cdot f_d} \cdot \overline{s}(t-\tau_i) = \sum_i \overline{A}_i \cdot e^{j2\pi\cdot\nu_i\cdot t} \cdot \overline{s}(t-\tau_i) \tag{2.6}$$

The motion of the receiver in combination with the i-th scatterer affects the received signal in amplitude and in the phase by the term $\overline{A}_i$, in the carrier frequency by the term ν_i and in the delay of the envelope by the term τ_i. The delay change of the envelope $v\cdot\cos(\gamma_i)t/c$ is too small that it can be ignored. Therefore motion of the receiver or a scatterer in the model introduces a frequency offset of the carrier in addition to the changes when no motion is involved.

When the number of the scatterers is very high, the discrete scatterer model has to be turned into a continuous scatterer model, where each specific scenario is represented by a gain density, given by the *delay-Doppler spread function* in Equation 2.7.

$$\overline{\varrho}(\nu,\tau)d\nu d\tau = \sum_{\hat{i}} \overline{A}_{\hat{i}} \tag{2.7}$$

Here index $\hat{i}$ refers to all scatterers with delay in $d\tau$ and Doppler shift in $d\nu$. With this we obtain the received signal $\overline{y}(t)$ given in Equation 2.8.

$$\overline{r}(t) = \int_0^{\infty} \int_{-f_d}^{f_d} \overline{\varrho}(\nu, \tau) \cdot e^{j2\pi \cdot \nu_i \cdot t} \cdot \overline{s}(t - \tau_i) \cdot d\nu d\tau \tag{2.8}$$

2.2.3. Characterization in Time and Frequency

The most harmful effects on the received signal in a multipath environment including motion are the frequency offset (Doppler shift) of the carrier and the time delay of the envelope. This is because these shifted and delayed waves might interfere destructively so that they cause severe attenuation. In practice a wireless transmission in a certain environment including a certain velocity of objects is described by the *Doppler spread* Δf_d and the *delay spread* $\Delta\tau$. Each path can be characterized by a different Doppler shift(due to a different receive angle) and time delay in both spreads result from multipath reception and also in the case of the Doppler spread caused from the mobility. While the Doppler spread is caused by the motion of objects within the environment (which might be the transmitter, the receiver or scatterers), the delay spread is caused only the topology of the environment itself. Although the Doppler spread is a phenomenon in frequency(generating Doppler shift, a shift in frequency), the overall result on the received signal, which is the result of interfering multiple Doppler shifted signal copies, is a time selective behavior. The situation is exactly opposite for the delay spread. While the delay spread is a phenomenon in time, the resulting effect on the received signal indicates a frequency selective behavior. This can be derived from the mathematical model introduced in the previous section. We first start with the discussion of the effect of the Doppler spread, then we discuss the impact of the delay spread.

Consider a receiver, moving through a multipath environment with a certain fixed velocity. All path delays in this environment are too small that can be ignored, therefore $s(t-\tau_i) \approx s(t)$. Then the received complex envelope, given by Equation 2.6, is simplified and turns into Equation 2.9.

$$\overline{r}(t) = \overline{s}(t) \cdot \sum_i \overline{A}_i \cdot e^{j2\pi \cdot \cos(\gamma_i) \cdot t \cdot f_d} = \overline{s}(t) \cdot \overline{h}(t) \tag{2.9}$$

Here $\overline{h}(t)$ is called the *complex gain* of the channel. In this case, the input $\overline{s}(t)$ and the output $\overline{r}(t)$ of the channel are connected by a simple multiplicative relationship. Since the phase angles $j2\pi \cdot \cos(\gamma_i) \cdot t \cdot f_d$ change in time, the complex gain of the channel is time varying. If a pure tone($\overline{s}(t) = U$) is transmitted through this channel, then the

received signal would be spread out in frequency, thus it is the shifted version of the transmitted signal within the interval $[-f_d, f_d]$. Due to this spreading, the received signal $\overline{r}(t)$, consists several tones at different frequencies interfering at the receiver, vary in time. Therefore the wireless channel is called *time selective* according to symbol time. At some instances the received signal is not attenuated and could appear even enhanced, while at other time instances the signal is severely attenuated. As a consequence, $\overline{h}(t)$ varies in time.

The time span which the receiver needs to process the incoming envelope indicates the severity of the time selective behavior of the channel. In general, the processing time span is represented by $N \cdot T_s$ where T_s denotes the symbol length. If the fade rate of the time selective process given by the Doppler frequency f_d is larger than the processing rate given by $\frac{1}{N \cdot T_s}$, then the fading process is called *time selective*. In contrast, if the fade rate is much lower than the processing rate, $f_d \cdot N \cdot T_s \ll 1$, then the fading process is called *not time selective*. These two conditions are also named *fast fading* and *slow fading*, respectively.

Now let us consider the impact of delay spread, without the presence of Doppler spread. For a stationary receiver, the phases of the reflected copies can be assumed constant. So we can consider Equation 2.10 as a mathematical model.

$$\overline{r}(t) = \sum_i \overline{A}_i \cdot \overline{s}(t - \tau_i) = \overline{h}(t) * \overline{s}(t) \tag{2.10}$$

In this case the input is related to the output by convolution with the complex gain $\overline{h}(t)$. Since the phases are constant(but still random), the channel can be modelled in this case as linear time invariant filter with an impulse response given in Equation 2.11.

$$\overline{h}(t) = \sum_i \overline{a}_i \cdot e^{-j\varphi_i} \cdot \delta(t - \tau_i) = \sum_i \overline{A}_i \cdot \delta(t - \tau_i) \tag{2.11}$$

The relationship between the input $\overline{S}(f)$ and the output $\overline{R}(f)$ in the frequency domain is given by multiplication of the input with the frequency response of the filter, the *complex transfer function* $\overline{H}(f)$. The transfer function is given in Equation 2.12.

$$\overline{H}(f) = \sum_i \overline{A}_i \cdot e^{-j2\pi \cdot f \cdot \tau_i} \tag{2.12}$$

Since the delays τ_i are different for several paths, some frequencies are attenuated

while the others not. If the delay difference between the paths is very small or even not existing, then there is no frequency attenuation caused by the delay spread. The severity of the delay spread can be indicated by the product of the required baseband bandwidth of the signal (denoted by W, and related to the symbol time T_s) and the delay spread. If the delay spread is very small compared to the symbol time T_s, then there is no impact on the received signal(if $\Delta\tau \cdot W \ll 1$). In this case the transfer function of the channel does not attenuates the signal significantly within the bandwidth of the signal W. This time the fading is called *flat or frequency non selective* because there is no signal attenuation for the utilized frequencies of the channel due to the delay spread. On the other hand if the delay spread is significant compared to the symbol time T_s, then the channel has a frequency selective behavior. That is, at some frequencies the received signal is attenuated while at other frequencies the signal might be enhanced. In this case the phenomenon called intersymbol interference occurs at the receiver. For instance, if the delay spread is half of the symbol time, then the signal copies of two consecutively transmitted symbols interfere at the receiver, such that the 'fast' signal copy of the latter transmitted symbol interferes with the 'slow' signal copy of the previous transmitted symbol. In Table 2.1 categories in order to characterize the fading of a wireless channel depending on the Doppler and delay spread are provided.

Table 2.2 gives typical ranges for the standard deviation of the delay spread. Note that mean values of the mentioned environments are negligible, because the variation of delays damage the signal, not a longer or shorter delay.

In practical situations both Doppler and delay spread are present most of the time. As a consequence a channel can be categorized into four different types, always depending on the ratios mentioned.

If both kinds of spread are present, then the channel has to be modelled as *linear time variant filter* (the filter model is necessary due to the delay spread, the time variant behavior is due to the Doppler spread). In this case input output relationship of the channel is given by Equation 2.13.

$$\overline{y}(t) = \sum_i \overline{A}_i \cdot e^{j2\pi\cdot\nu_i\cdot t} \cdot \overline{s}(t-\tau_i) = \overline{h}(t,\tau) * \overline{s}(t) = \int_0^{\Delta\tau} \overline{h}(t,\tau)\cdot\overline{s}(t-\tau)d\tau \quad (2.13)$$

The impulse response of the channel is given by Equation 2.14.

Table 2.1. Categories in order to characterize the fading of a wireless channel depending on the Doppler and delay spread

Criteria	**Category**
$\frac{\Delta\tau}{T_s} \ll 1$, $f_d \cdot T_s \ll 1$	not frequency selective (flat), not time selective (slow)
$\frac{\Delta\tau}{T_s} \gg 1$, $f_d \cdot T_s \ll 1$	frequency selective, not time selective (slow)
$\frac{\Delta\tau}{T_s} \ll 1$, $f_d \cdot T_s \gg 1$	not frequency selective (flat), time selective (fast)
$\frac{\Delta\tau}{T_s} \gg 1$, $f_d \cdot T_s \gg 1$	frequency selective, time selective

Table 2.2. Standard deviation of delay spread values for three often referred transmission environments

Environment	τ_{rms}
Urban	1 - 25 μs
Suburban	0.2 - 2 μs
Indoor	25 - 250 ns

$$\overline{h}(t,\tau) = \sum_i \overline{A}_i \cdot e^{j2\pi\cdot\nu_i\cdot t} \cdot \delta(t-\tau_i) \tag{2.14}$$

In the frequency domain input output relationship is given by Equation 2.15.

$$\overline{Y}(f) = \overline{H}(t,f)\cdot\overline{S}(f) = \left(\sum_i \overline{A}_i \cdot e^{j2\pi\cdot\nu_i\cdot t}\cdot e^{-j2\pi\cdot f\cdot\tau_i}\right)\cdot\overline{S}(f) \tag{2.15}$$

Here $\overline{H}(t,f)$ denotes the time variant transfer function and determines the gain experienced at time t to a frequency component at frequency f.

2.2.4. First Order Statistics of Fading

In general a received signal consists of a large number of signal copies which interfere at receive antenna. If all channel coefficients were known at each time instance, the wireless channel could be seen as a deterministic channel in principle. Due to the large number of reflection paths this is not possible in practice. Therefore a statistical description is the only way to characterize at least some properties of the channel.

Since there is high number of signal paths existing in a usual propagation environment, the *central limit theorem* may be applied to the statistical behavior of the interfering signal copies at the receiver. If the number of paths tends to infinity, then the fading can be modeled by complex white Gaussian process. As a consequence, if Doppler spread is present and there is high number of signal copies interfering, then the complex gain $\overline{h}(t)$ can be modelled as Gaussian random process in time. If delay spread is present, the complex transfer function $\overline{H}(f)$ can be modelled as Gaussian random process in frequency. If both kinds of spread are present, the time variant transfer function $\overline{H}(t, f)$ in other words, the Fourier transform of the time variant impulse response can be modelled as Gaussian random process in both time and frequency.

Let us consider the complex gain is Gaussian (in the case of flat fading and the absence of a line of sight component), the probability density function of the complex gain $\overline{h}(t)$ is given by Equation 2.16.

$$p(|\overline{h}|) = \frac{1}{2\pi\sigma_h^2} \cdot e^{-\frac{(|\overline{h}|)^2}{\sigma_h^2}} \tag{2.16}$$

The variance σ_h^2 is given by Equation 2.17 where $\overline{h}_r(t)$ and $\overline{h}_i(t)$ denotes real and imaginary parts of the complex Gaussian random process $\overline{h}(t)$ respectively. Also this process has zero mean.

$$\sigma_h^2 = \frac{1}{2} \cdot E(|\overline{h}(t)|^2) = \frac{1}{2} \cdot E(\overline{h}_r(t)^2) + \frac{1}{2} \cdot E(\overline{h}_i(t)^2) \tag{2.17}$$

If we change Cartesian coordinates to polar coordinates ($\overline{h} = \overline{h}_r + \overline{h}_i = r \cdot e^{j\theta}$) by standard transformation then we obtain the following joint probability density function in Equation 2.18.

$$p(r, \theta) = \frac{r}{2\pi \cdot \sigma_h^2} \cdot e^{\frac{-r^2}{2\sigma_h^2}} \tag{2.18}$$

Since r and θ are independent, where θ has a uniform distribution, then the distribution of r is called Rayleigh distribution and probability density function of this distribution is given by Equation 2.19.

$$p(|\overline{h}(t)|) = p(r) = \frac{r}{\sigma_h^2} \cdot e^{\frac{-r^2}{2\sigma_h^2}} \tag{2.19}$$

This form of fading is characterized by the absence of a line of sight component,

which is a very strong and 'fast' path compared to all other paths. The pdf of this function is plotted in Figure 2.2. The instantaneous power has to be obtained for determining the

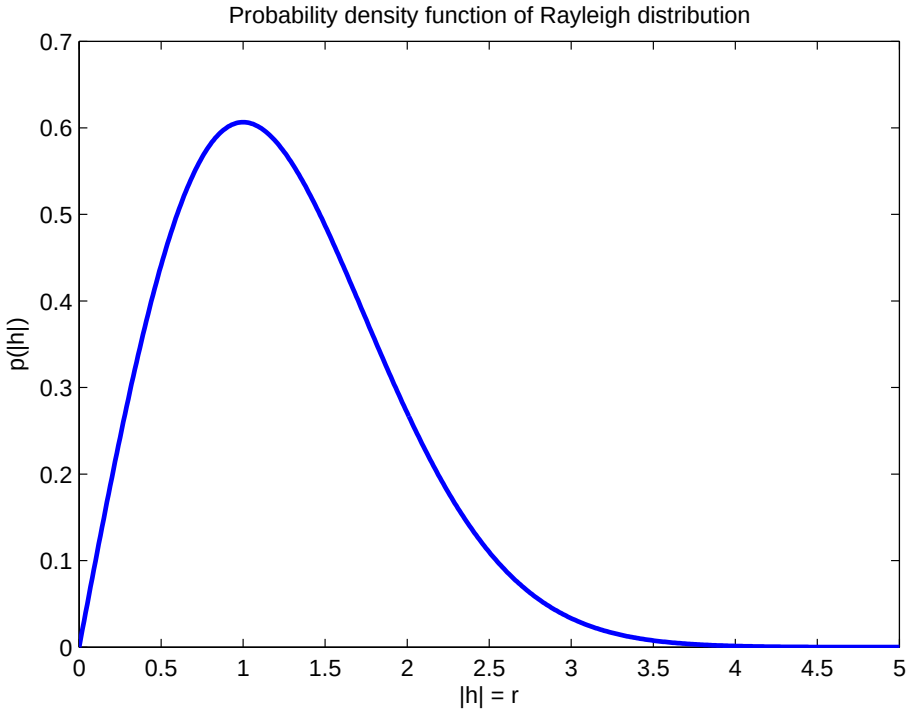

Figure 2.2. Probability Density Function of the Rayleigh Distribution

actual SNR at the receiver rather than the instantaneous amplitude. This is given by the squared amplitude $z = r^2 = |\overline{h}|^2$ and the distribution of z is actually χ^2 distribution with two degrees of freedom. This is due to the two independent jointly Gaussian random process of the real and imaginary parts of the signal combining. The probability density function of z is determined by Equation 2.20.

$$p(|\overline{h}(t)|^2) = p(z) = \frac{1}{2\sigma_h^2} \cdot e^{\frac{-z}{2\sigma_h^2}} \tag{2.20}$$

In the case of existing line of sight component, the distribution of r is no longer Rayleigh but *Rician*, since one distinct path dominates. In other words it is received much stronger (in terms of power) than the remaining paths. In such a situation, random multi-path components arriving at different angles are superimposed on a stationary dominant signal. At the output of an envelope detector, this has the effect of adding dc component to the random multipath.

The Rician distribution depends on the ratio between the power of the strong path

and the power of the remaining paths. Therefore this distribution can characterize many different line of sight scenarios while the Rayleigh distribution only characterize the non-line of sight situation.

The probability density function of the Rician distribution is given by the Equation 2.21.

$$p(r) = \begin{cases} \frac{r}{\sigma_h^2} \cdot e^{-\frac{(r^2+A^2)}{2\sigma_h^2}} \cdot I_0(\frac{Ar}{\sigma_h^2}) & A \geq 0, r \geq 0 \\ 0 & r < 0 \end{cases} \tag{2.21}$$

The parameter A denotes the peak amplitude of the dominant signal and $I_0(\cdot)$ is the zero-order modified Bessel function of the first kind. The Rician distribution is often described in terms of a parameter K which is defined as the ratio between the deterministic signal power and the variance of the multipath. This parameter is given by $K = A^2/(2\sigma_h^2)$, or in terms of dB

$$K(dB) = 10\log(\frac{A^2}{2\sigma_h^2})dB \tag{2.22}$$

The parameter K is known as the Rician factor and completely specifies the Rician distribution. As $A \longrightarrow 0, K \longrightarrow -\infty$ dB, and as the dominant path decreases in amplitude, the Rician distribution degenerates to a Rayleigh distribution.

For small number of paths (< 5), the central limit theorem does not hold any more, so Gaussian process assumption does not fit adequately (Cavers 2000). In this case the amplitude of r of the received signal can be modelled by *Nakagami* distribution. The instantaneous power z of the signal has a Γ distribution. Addition to this by varying a variable m the Nakagami distribution can take into account the absence or presence of a line of sight. Also the Nakagami distribution is more convenient for analytical work. For detailed derivation and discussion refer to (Cavers 2000).

As already mentioned, the Rayleigh distribution occurs in most non-line of sight settings, which are encountered mostly with indoor scenarios as well as with microcells in urban areas. Rician distribution are seen on the opposite environments where Rayleigh fading occurs (refer to (Cavers 2000)). However, by considering Rayleigh fading, one is working with the worst possible scenario, since the Rician fading is less destructive and the performance of the communication system is better.

2.2.5. Second Order Statistics of Fading

In order to describe a Gaussian random process it is sufficient to know its mean and its autocorrelation function, or *power spectrum* which is the Fourier transform of autocorrelation function. We have already shown the mean implicitly in the previous Section. In this Section we desire to obtain the second order description of the process in case of the Doppler spread as well as in the case of delay spread.

In the case of Doppler spread only, where $s(t-\tau_i) \approx s(t)$, the received signal $\overline{r}(t)$ is determined by the product of the transmitted signal $\overline{s}(t)$ and the complex gain of the channel $\overline{h}(t)$ where the complex gain of the channel is time variant. If a pure tone is transmitted through the channel then the received signal consists of multiple tones at frequencies in the vicinity of the carrier with a maximum shift of the Doppler frequency f_d.

Let us consider a mobile receiver moving with the velocity v in a multipath environment. Each Doppler frequency ν is given by Equation 5.7.

$$\nu = f_d \cdot cos(\gamma) \tag{2.23}$$

Generally ν varies from $+f_d$, resulting from reflected paths in front of the receiver, to $-f_d$, resulting from reflected paths behind the receiver (behind and in front relate to the direction of movement of the receiver). Since $\cos(\cdot)$ is an even function, the Doppler shift frequency varies from a scattering angle of $-\gamma$ or γ. If we differentiate Equation 5.7 then we obtain the relationship between (small) ranges of ν and of the angle γ in Equation 2.24

$$\frac{d\nu}{d\gamma} = f_d \cdot \sin(\gamma) = f_d \cdot \sqrt{1-\cos(\gamma)^2} = f_d \cdot \sqrt{1-\left(\frac{\nu}{f_d}\right)^2} \tag{2.24}$$

Assume that there is high number of scatterers, therefore the power received from differential angle $d\gamma$ is given by the product of power density $P(\gamma)$ and differential angle $d\gamma$. Thus we can relate the received power $S_{\overline{h}}$ to the Doppler shift frequency ν and with this we obtain the received *power spectrum* $S_{\overline{h}}(\nu)$.

$$S_{\overline{h}}(\nu) = \frac{P(\gamma)+P(-\gamma)}{f_d \cdot \sqrt{1-\left(\frac{\nu}{f_d}\right)^2}} \tag{2.25}$$

If we consider the special case of *isotropic scattering*, implying that the power

received from different angles is equivalent ($P(\gamma) = \frac{\sigma_{\bar{h}}^2}{2\pi}$). In this case the Equation 2.25 turns into Equation 2.26.

$$S_{\bar{h}}(\nu) = \frac{(\sigma_{\bar{h}})^2}{\pi \cdot f_d} \cdot \frac{1}{\sqrt{1 - \left(\frac{\nu}{f_d}\right)^2}} \tag{2.26}$$

This is well known U shaped spectrum shown in Figure 2.3 , and it is often referred to as *Jakes' spectrum*.

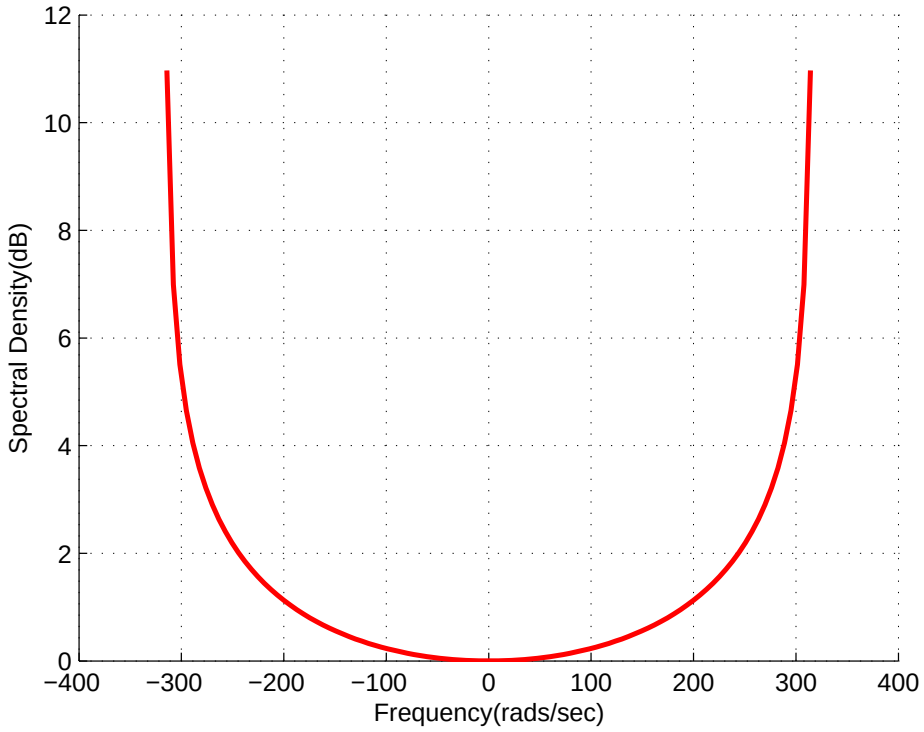

Figure 2.3. Power spectrum for the isotropic scattering case

We can easily derive the autocorrelation function of the complex channel gain by taking inverse Fourier transform of the power spectrum given in Equation 2.27

$$\begin{aligned} r_{\bar{h}}(\tau) &= \int_{-f_d}^{f_d} S_{\bar{h}}(\nu) \cdot e^{j2\pi \cdot \nu \cdot \tau} d\tau = \frac{\sigma_{\bar{h}}^2}{2\pi} \cdot \int_{-\pi}^{\pi} e^{j2\pi \cdot f_d \cdot \cos(\gamma)\tau} d\gamma \\ &= \sigma_{\bar{h}^2} J_0(2\pi f_d \tau) = \sigma_{\bar{h}^2} J_0(2\pi \frac{x}{\lambda}) \end{aligned} \tag{2.27}$$

The function $J_0(\cdot)$ denotes the zeroth-order Bessel function of the first kind. Equation 2.27 relates the autocorrelation function which depends on time difference τ with a space difference x.

Table 2.3. Coherence time values for different carrier frequencies at various speeds

Carrier Frequency	T_c@1 m/s	T_c@10 m/s	T_c@20 m/s	T_c@100 m/s
1 MHz	68.2 s	6.82 s	3.41 s	0.68 s
100 MHz	0.68 s	68.2 ms	34.1 ms	6.82 ms
1 GHz	68.2 ms	6.82 ms	3.41 ms	0.68 ms
2.4 GHz	28.1 ms	2.81 ms	1.4 ms	0.28 ms
5.4 GHz	12.5 ms	1.25 ms	0.62 ms	0.12 ms
10 Ghz	6.82 ms	0.68 ms	0.34 ms	68.2 μs
60 Ghz	1.12 ms	0.11 ms	56.2 μs	11.2 μs

If we assume that the scatterers at different Doppler shifts ν are uncorrelated, then $\overline{h}(t)$ is in fact uncorrelated. This assumption is called the *wide sense stationary (WSS)* assumption and given in Equation 2.28.

$$E[\overline{h}(t)\overline{h}^{*}(t-\tau)] = r_{\overline{h}}(\tau) \tag{2.28}$$

From the autocorrelation function, one can derive a measure in time characterizing the channel encountered. This is called the *coherence time* and indicates the time span that channel roughly stays constant. One mathematical definition of the coherence time is determined by Equation 2.29 which equals an autocorrelation value of 0.98 (Cavers 2000). But this definition is somewhat subjective and other definitions can be found in literature (Proakis 2001), (Rappaport 1999), (Steele 1992).

$$T_c = \frac{1}{2\pi \cdot \nu_{rms}} = \frac{1}{\sqrt{2}\pi f_d} \tag{2.29}$$

In (2.29) ν_{rms} denotes the standard deviation of the power spectrum $S_{\overline{h}}(\nu)$ given by Equation 2.26. For the case of isotropic scattering the variance is $\nu_{rms} = \frac{f_d}{\sqrt{2}}$. Typical values for the coherence time are given in Table 2.3. As long as the required bandwidth is much smaller than the carrier frequency, it has no effect. If the required bandwidth is not significantly smaller compared to the carrier frequency, the expected coherence time equals the coherence time of the highest frequency involved in the communication scheme.

In the presence of only delay spread the wireless channel can be modeled as linear time invariant filter. Thus the received signal $\overline{y}(t)$ is determined by the convolution of the transmitted signal $\overline{s}(t)$ and the channel impulse response $\overline{h}(t)$. Accordingly, the received signal in the frequency domain is given by the product of the Fourier transform of the transmitted signal and the transfer function $\overline{H}(f)$ of the channel. We desire to obtain a spaced frequency correlation function of $\overline{H}(f)$, that is a function giving us the correlation between the transfer function at different frequencies. In general this function is given by:

$$\overline{r}_{\overline{H}}(f, f - \Delta f) = \frac{1}{2} \cdot E[\overline{H}(f) \cdot \overline{H}^{*}(f - \Delta f)] \tag{2.30}$$

If we substitute Equation 2.12 into Equation 2.30 then we have

$$\overline{r}_{\overline{H}}(f, f - \Delta f) = \frac{1}{2} \cdot E\left[\sum_{i}\sum_{k} \overline{A}_i \overline{A}_k^{*} \cdot e^{-2\pi j f(\tau_i - \tau_k)} \cdot e^{-2\pi j \Delta f \tau_k}\right]. \tag{2.31}$$

If scatterers at different delays are uncorrelated, this autocorrelation function depends only on the frequency difference Δf. This assumption is called the *uncorrelated scatterers (US) assumption* of wireless channels.

$$\frac{1}{2} \cdot E\left[\sum_{i}\sum_{k} \overline{A}_i \overline{A}_k^{*}\right] = \frac{1}{2} \cdot E\left[\sum_{k_i} \overline{A}_i \overline{A}_k^{*}\right] = \sigma_i \tag{2.32}$$

Here k_i indicates the scatterers with the same delay τ_i. Using this identity Equation 2.31 turns into

$$\overline{r}_H(\Delta f) = \sum_{k} (\sigma_k)^2 \cdot e^{-2\pi j \Delta f \tau_k} \tag{2.33}$$

If there are a lot of scatterers then this summation becomes a density depending on the delay τ. This density is called the *power delay profile* given by

$$\overline{r}_H(\Delta f) = \int_0^{\infty} P(\tau) \cdot e^{-2\pi j \Delta f \tau} \cdot d\tau. \tag{2.34}$$

Exponential profile, which is one idealized but often used function for the power delay profile is given by

$$P(\tau) = \frac{(\sigma_{\overline{h}})^2}{\tau_{rms}} \cdot e^{-\frac{\tau}{\tau_{rms}}} \tag{2.35}$$

$(\tau_{rms})^2$ is the delay variance and the square root of this, the standard deviation of the delay, is an often used measure for the delay spread of a propagation environment. The delay variance is obtained by

Table 2.4. Coherence Bandwidth ranges for three typical environments

Environment	W_c
Urban	6.4 kHz - 160 kHz
Suburban	80 kHz - 800 kHz
Indoor	0.64 MHz -6.4 MHz

$$\tau_{rms}^2 = \frac{1}{\sigma_{\bar{h}^2}} \cdot \int_0^\infty (\tau - \tau_m)^2 \cdot P(\tau) d\tau. \tag{2.36}$$

τ_m denotes the mean delay and is given by

$$\tau_m = \frac{1}{\sigma_{\bar{h}}^2} \cdot \int_0^\infty \tau \cdot P(\tau) d\tau. \tag{2.37}$$

For the exponential power delay profile τ_{rms} equals τ_m.

From the autocorrelation function of the transfer function of the wireless channel with uncorrelated scatterers a measure in frequency can be derived characterizing the channel encountered. The meaning of this measure is related to the coherence time and is called the *coherence bandwidth*. The coherence bandwidth measures the frequency spacing roughly for which the channel does not change significantly. Again the exact mathematical definition is somewhat subjective. One definition of the coherence bandwidth is given in (Cavers 2000)

$$W_c = \frac{1}{2\pi\tau_{rms}}. \tag{2.38}$$

Other definitions can be found in (Proakis 2001), (Rappaport 1999), (Steele 1992).

In Table 2.4 ranges of the coherence bandwidth are given for different environments. Note that the carrier frequency does not affect the coherence bandwidth. If the coherence bandwidth is much smaller than the required bandwidth for transmission, the system will suffer from intersymbol interference (ISI), no matter at which carrier frequency the system is working. Therefore, it is much easier to communicate at high data rates in indoor scenarios due to the large coherence bandwidth than in urban environments, here ISI degradates the performance severely. Now let us consider the case where both effects present at the same time. First recall the input output relationship in the case

of many scatterers given by Equation 2.8.

$$\overline{r}(t) = \int_0^{\infty} \int_{-f_d}^{f_d} \overline{\varrho}(\nu, \tau) \cdot e^{j2\pi \cdot \nu_i \cdot t} \cdot \overline{s}(t - \tau_i) \cdot d\nu d\tau$$

If we observe the output in the case of a single carrier input at frequency f, where $s(t) = e^{2\pi j \cdot f \cdot t}$, we obtain the output given by:

$$\overline{r}(t) = \int_0^{\infty} \int_{-f_d}^{f_d} \overline{\varrho}(\nu, \tau) \cdot e^{j2\pi \cdot \nu_i \cdot t} e^{-2\pi j f t} \cdot e^{-2\pi j f \tau} \cdot d\nu d\tau = e^{2pijft} \cdot \overline{H}(t, f) \qquad (2.39)$$

Here $\overline{H}(t, f)$ is the time variant transfer function and determines the complex gain at frequency f at time t. Since both delay and Doppler spread are now present, we want to obtain a time-frequency correlation function of $\overline{H}(t, f)$. That is a function representing the correlation between the complex gain at time t and at frequency f, compared to the complex gain at time $t + \Delta t$ and at frequency $f + \Delta f$.

Considering the WSS assumption (scatterers at different Doppler shifts are uncorrelated) and the US assumption (scatterers at different delays are uncorrelated), this desired function only depends on the delay and the frequency differences present.

$$r_{\overline{H}}(\Delta t, \Delta f) = \int_{-\infty}^{\infty} \int_{-\infty}^{\infty} S_{\overline{\varrho}(\nu,\tau)} \cdot e^{2\pi j \nu \Delta t} \cdot e^{2\pi j \Delta f \tau} d\nu d\tau. \qquad (2.40)$$

In this equation $S_{\overline{\varrho}(\nu,\tau)}$ is called the *delay-Doppler power density function* or also the *scattering function*. It represents the power density of the environment at Doppler shift ν and delay τ. This function is related to the power delay profile by

$$P(\tau) = \int_{-\infty}^{\infty} S_{\overline{\varrho}}(\nu, \tau) d\nu. \qquad (2.41)$$

It is related to the Doppler spectrum by integrating the scattering function in the delay domain.

In order to determine the functional behavior of the scattering function assume that the Doppler spectrum is not linked to the delay profile. Then the scattering function is called to be *separable*.

$$S_{\overline{\varrho}}(\nu, \tau) = \frac{S_{\overline{\varrho}}(\nu, \tau) \cdot P(\tau)}{\sigma^2_{\overline{h}}} \qquad (2.42)$$

With this assumption, the Equation 2.40 becomes simpler and turns into

$$r_{\overline{H}}(\Delta t, \Delta f) = \frac{r_{\overline{h}}(\Delta t) \cdot r_{\overline{H}}(\Delta f)}{\sigma^2_{\overline{h}}}. \qquad (2.43)$$

CHAPTER 3

SIMULATION MODELS FOR FADING CHANNELS

It is important to simulate communication systems in software for system design and verification. Simulation offers cost effective and time saving alternative to real time testing in the field. The prime requirement of the simulation set-up is to capture the fading effects created by a radio channel. As a result, efforts have been made to develop efficient models to simulate the actual radio propagation environment in software and test various communications algorithms. There are several methods in the communications literature to simulate Rayleigh fading. This methods can be based on either sum of sinusoids principle or filtering of the white Gaussian noise. Our proposed simulation model is also based on filtering of the white Gaussian noise. Before we discuss our contributions in this area, it is necessary to understand different simulation philosophies commonly employed to simulate fading channels. Therefore, we provide an overview of different simulation techniques in this chapter. Specifically, we discuss the sum of sinusoids models and different kinds of filtered noise models along with their pros and cons.

3.1. Sum of Sinusoids Models

Complex channel envelope of multipath fading channel can be represented as a sum of homogeneous wave components. Each homogenous component is represented by a complex sinusoid with certain amplitude, frequency, and phase. The overall channel waveform is the sum of several sinusoids. Therefore, this channel description is often called a ”sum-of-sinusoids” model. Being a natural representation of the channel waveform, several sum of sinusoids models have been presented in the past to simulate wireless channels. Rather than simulating the channel by directly applying the Clarke’s reference model (Clarke 1968), specialized sum of sinusoids models are proposed to efficiently simulate the channel by using a finite number of sinusoids. The philosophy of sum of sinusoids modeling has been made popular by the pioneering work of Jakes (Jakes 1974), which is discussed below.

For convenience, first we discuss the Clarke’s reference model. Clarke’s model

defines the complex channel gain under non-line of sight, frequency flat fading, and 2-D isotropic scattering assumptions as (Clarke 1968)

$$h(t) = \sqrt{\frac{2}{N}} \sum_{n=1}^{N} e^{j[2\pi f_d t \cos(\alpha_n) + \phi_n]} \tag{3.1}$$

where N denotes the number of propagation paths, $\phi_n \sim U[-\pi, \pi)$ and $\alpha_n \sim U[-\pi, \pi)$ are the random phase and angle of arrival of the n^{th} multipath component respectively, and f_d is the maximum Doppler frequency due to the mobility of the receiver. To simulate the wireless channel, this sum of sinusoids model can be applied directly by generating the random variables involved in the model. However, this high degree of randomness is not desirable for efficient simulation. Therefore Jakes proposed the following sum of sinusoids model:

$$h_I(t) = \sqrt{2}\cos(2\pi f_d t) \cdot 2 \sum_{n=1}^{M} \cos\left(\frac{2\pi n}{M}\right) \cos\left(2\pi f_d \cos\left[\frac{2\pi n}{4M+2}\right] t\right) \tag{3.2}$$

$$h_Q(t) = 2 \sum_{n=1}^{M} \sin\left(\frac{2\pi n}{M}\right) \cos\left(2\pi f_d \cos\left[\frac{2\pi n}{4M+2}\right] t\right) \tag{3.3}$$

where $h_I(t)$ and $h_Q(t)$ denotes the in-phase and quadrature phase components of the complex channel gain and M denotes the number of sinusoids. A detailed discussion about derivation of the model parameters can be found in (Jakes 1974), (Stüber 2001). The intuition behind this model is the fact that under 2-D isotropic scattering, the symmetry in the environment can be exploited to reduce the number of sinusoids. For instance, while the Clarke's model distributes the angles of arrival over $[-\pi, \pi)$ resulting in negative as well as positive Doppler frequencies in the model, the Jakes' model simulates only the positive Doppler frequencies to reduce the number of sinusoids M. The amplitudes of these sinusoids, i.e., $\cos(\alpha_n)$ and $\sin(\alpha_n)$ are chosen to produce zero cross-correlation between the in-phase and quadrature components, a constraint imposed by the Clarke's model to generate Rayleigh faded envelope.

The Jakes' model has been the de-facto simulation model for a long time. However, recent studies have highlighted several drawbacks (Young and Beaulieu 2001), (Zheng and Xiao 2002) of this model. It was shown in (Young and Beaulieu 2001) that the fading signals which are produced by classical Jakes simulator are not wide-sense stationary (WSS). Also, since all the parameters in the model are fixed (deterministic),

the channel gains simulated in each simulation run is identical. Therefore, statistical averaging or Monte Carlo simulation results cannot be obtained while computing metrics such as bit error rate (BER).

Several statistical methods have been proposed by Zheng and Xiao (Xiao and Zheng 2002), (Zheng and Xiao 2002), (Zheng and Xiao 2003), (Zheng, et al. 2003) for wireless channels to remove this drawback. These methods differ from one another in terms of the model parameters and therefore they have different time-average properties. In this thesis we simulate and make performance and complexity analysis of one of the method's proposed in (Zheng and Xiao 2002). With this method the normalized low-pass discrete Rayleigh fading process is generated by

$$h[n] = h_I[n] + jh_Q[n], \tag{3.4a}$$

$$h_I[n] = \frac{1}{\sqrt{N_s}} \sum_{k=1}^{N_s} \cos(2\pi f_m n \cos \alpha_k + \phi_k) \tag{3.4b}$$

$$h_Q[n] = \frac{1}{\sqrt{N_s}} \sum_{k=1}^{N_s} \cos(2\pi f_m n \sin \alpha_k + \varphi_k) \tag{3.4c}$$

with

$$\alpha_k = \frac{2\pi k - \pi + \theta}{4N_s}, \quad k = 1, 2, \cdots, N_s \tag{3.5}$$

where ϕ_k, φ_k and θ are statistically independent and uniformly distributed on $[-\pi, \pi)$ for all k and N_S denotes the number of sinusoids.

3.2. Filtered Gaussian Noise Models

Ultimately, the goal of any simulation model is to reproduce the channel properties. Therefore, in contrast to sum of sinusoids models, filtered Gaussian noise models are adapted to simulate the channel properties by means of signal processing techniques without considering the underlying propagation mechanism. Instead of adding sinusoids to generate fading, these models filter Gaussian noise to generate the complex channel gains. The underlying principle is that on filtering Gaussian noise through appropriately designed filters, the channel power spectral density (psd or the Doppler spectrum) can be simulated, thereby capturing the important first and second order fading statistics.

To understand the working of filtered noise models, first we discuss an important result obtained from the linear time invariant filtering theory. Given a filter with frequency

response $H(f)$, if a signal $x(n)$ with psd $P_{xx}(f)$ is filtered through this filter, the output $y(n)$ has psd given by

$$P_{yy}(f) = P_{xx}(f)|H(f)|^2. \tag{3.6}$$

To generate the Gaussian in-phase or quadrature components of the complex channel coefficients, each having a Doppler spectrum $P_{yy}(f) = S(f)$, one can filter a white Gaussian random process with psd of $N_0/2$ through a filter $H(f)$ whose frequency response is chosen to be

$$H(f) = \sqrt{\frac{2}{N_0} S(f)}. \tag{3.7}$$

Then, the output random process will also be Gaussian with a psd of $S(f)$, thereby reproducing the properties of the complex Gaussian channel. The next goal in the simulation model is to implement the filter $H(f)$. We describe three such implementation schemes below - the Inverse Discrete Fourier Transform (IDFT) filter model (Young and Beaulieu 2000), the Autoregressive (AR) filter model (Baddour and Beaulieu 2005) and our proposed fading filter design. The IDFT filter method is designed in the frequency domain while our proposed filter design and the Autoregressive model are designed in time domain to provide an approximation of the Doppler spectrum that we desire.

3.2.1. IDFT Filter Design Method

Since it is easy to discuss the IDFT operation in discrete time, and our ultimate goal is to simulate discrete time waveforms, we deal with discrete time-domain sequences in this section. A block diagram of this method is shown in Figure 3.1. In

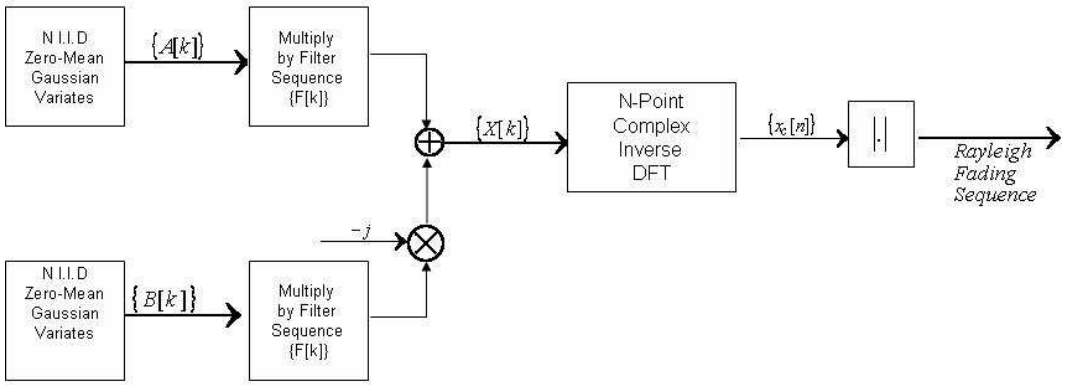

Figure 3.1. Block Diagram of the IDFT Method

this method, the IDFT operation is applied to complex sequences of independent, nor-

mally distributed random numbers, each sequence multiplied by suitable filter coefficients. To generate a discrete time sequence $y[n]$ of N complex Gaussian variables with a given Doppler spectrum, the Doppler spectrum is sampled at N equi-spaced frequencies $f_k = (kf_s)/(N), k = 0, 1, \ldots, N-1$ where f_s is the sampling frequency. The filter coefficients can be determined by Equation (3.8):

$$F[k] = \begin{cases} 0 & k = 0, \\ \sqrt{\frac{1}{2\sqrt{1-(\frac{k}{Nf_m})^2}}} & k = 1, 2, ..., k_m - 1, \\ \sqrt{\frac{k_m}{2}[\frac{\pi}{2} - \arctan(\frac{k_m - 1}{\sqrt{2k_m - 1}})]} & k = k_m, \\ 0, & k = k_m + 1, ..., N - k_m - 1, \\ \sqrt{\frac{k_m}{2}[\frac{\pi}{2} - \arctan(\frac{k_m - 1}{\sqrt{2k_m - 1}})]} & k = N - k_m, \\ \sqrt{\frac{1}{2\sqrt{1-(\frac{N-k}{Nf_m})^2}}} & k = N - k_m + 1, ..., N - 1. \end{cases} \tag{3.8}$$

where N denotes the number of symbols and $k_m = \lfloor (f_m N) \rfloor$. In addition, two sequences $A[k]$ and $B[k]$, each having N independent and identically distributed (iid) real Gaussian random variables with zero mean and variance σ^2 are generated. Then, the desired signal y[n] is obtained as

$$y[n] = IDFT\{A[k]F[k] - jB[k]F[k]\}. \tag{3.9}$$

3.2.2. Autoregressive Filter Model

The AR model imposes an all-pole structure on the filter $H(f)$ and determines the AR filter coefficients in the time-domain by using the knowledge of channel autocorrelation function. However, it must be noted that the underlying principle of filtering Gaussian noise to produce an output with the desired psd remains the same.

Autoregressive models are generally used to approximate discrete-time random processes. This is due to the simplicity of computing of their parameters and due to their correlation matching property. Let $x[n]$ be a white Gaussian random process filtered

through a p^{th} order (p poles) AR filter $H(z) = 1/A_k(z) = 1/(1 + \sum_{k=1}^{p} a_k z^{-1})$. Then, the output $y[n]$ is given by the difference equation

$$y[n] = -\sum_{k=1}^{p} a_k x[n-k] + x[n]. \tag{3.10}$$

The AR model parameters are the filter coefficients $\{a_1, a_2, \ldots, a_p\}$ and the variance σ_p^2 of the driving noise process $x[n]$. The corresponding power spectral density of the AR(p) process is given by (Baddour and Beaulieu 2005)

$$S_{yy}(f) = \frac{\sigma_p^2}{|1 + \sum_{k=1}^{p} a_k e^{-j2\pi fk}|^2} \tag{3.11}$$

Although the Doppler spectrum models proposed for mobile radio channel are not rational, an arbitrary spectrum can be closely approximated by a sufficiently large AR model order. The basic relationship between the desired model autocorrelation function $R_{yy}[k]$ and the AR(p) parameters is given by:

$$R_{yy}[k] = \begin{cases} -\sum_{m=1}^{p} a_m R_{yy}[k-m], & k \geq 1 \\ -\sum_{m=1}^{p} a_m R_{yy}[k-m] + \sigma_p^2, & k = 0. \end{cases} \tag{3.12}$$

In the matrix form this becomes for $k = 1, 2, \cdots, p$

$$\mathbf{R_{yy}a} = -\mathbf{v}, \tag{3.13}$$

where

$$\mathbf{R_{yy}} = \begin{bmatrix} R_{yy}[0] & R_{yy}[-1] & \cdots & R_{yy}[-p+1] \\ R_{yy}[1] & R_{yy}[0] & \cdots & R_{yy}[-p+2] \\ \vdots & \vdots & \ddots & \vdots \\ R_{yy}[p-1] & R_{yy}[p-2] & \cdots & R_{yy}[0] \end{bmatrix},$$

$\mathbf{a} = [a_1, a_2, \cdots, a_p]^T$,$\mathbf{v} = [R_{yy}[1], R_{yy}[2], \cdots, R_{yy}[p]]^T$, and

$$\sigma_p^2 = R_{yy}[0] + \sum_{k=1}^{p} a_k R_{yy}[k]. \tag{3.14}$$

Given the desired autocorrelation sequence, the AR filter coefficients can be determined by solving the set of p Yule-Walker equations. These equations can in principle be solved by the Levinson-Durbin recursion. However, an exact solution to the Yule-Walker equation does not exist if the autocorrelation matrix $\mathbf{R_{yy}}$ is non-singular and therefore non-invertible. In such cases, a solution is obtained by using a technique called diagonal

loading or matrix stabilization, where we artificially introduce some noise variance into $\mathbf{R_{yy}}$ to make it stable, non-singular and thus invertible matrix. Then AR fading filter coefficients can be obtained by:

$$\mathbf{a_k} = -(\mathbf{R_{yy}} + \epsilon\mathbf{I})^{-1}\mathbf{v}, \tag{3.15}$$

where $\mathbf{I}$ is a $p \times p$ identity matrix and $\epsilon \neq 0$ is a suitable diagonal loading parameter that renders $(\mathbf{R_{yy}} + \epsilon\mathbf{I})$ non singular and invertible.

3.2.3. Our Proposed Fading Filter Design

A straightforward method to simulate a faded signal is to amplitude modulate the carrier signal with a low-pass filtered Gaussian noise source as shown in Figure 3.2. If the

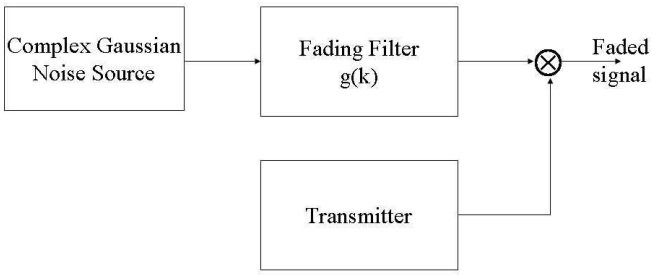

Figure 3.2. Faded signal generator that uses low-pass filtered white complex Gaussian noise

Gaussian noise sources have zero-mean then this method produces a Rayleigh faded envelope (Stüber 2001). In order to obtain time varying frequency selective fading channel we must have a bank of these fading filters where each filter generates the corresponding fading channel tap. A fading filter with impulse response $g(k)$ can be designed so that its output spectral density is an approximation to theoretical spectral density of the complex envelope of the faded signal $S(f)$. Consider the elementary first order filter transfer function $G_1(s)$, and the second order filter transfer function $G_2(s)$ where

$$G_1(s) = \frac{w_x}{s + w_x}, \tag{3.16}$$

and

$$G_2(s) = \frac{w_x^2}{s^2 + \frac{w_x s}{Q} + w_x^2}. \tag{3.17}$$

Then we can have fading filter continuous time transfer functions with higher orders (of order γ), $G_\gamma(s)$, that are given by

$$G_\gamma(s) = \begin{cases} G_2^{\gamma/2}(s), & \text{if } \gamma \text{ even}, \\ G_1(s)G_2^{(\gamma-1)/2}(s), & \text{if } \gamma \text{ odd}, \end{cases} \tag{3.18}$$

where $G_1(s)$ and $G_2(s)$ are as given by (3.16) and (3.17) respectively, and the selection of Q is such that there is a pre-specified frequency response level at $w = w_x$ rad/sec; for example for the third-order filter if $Q = \sqrt{10}$ then the magnitude of $G(\cdot)$ will have a gain of 7dB at $w = w_x$ (10dB gain from the second order filter and -3dB from the first order part making the overall gain of 7dB). In order to find the parameters of the fading filter transfer function, $G_\gamma(s)$, we will first set the filter order γ and Q. Then defining $S(f;\epsilon)$, as an approximation to the theoretical spectral density of (Jakes 1974), by

$$S(f;\epsilon) = \begin{cases} \frac{\sigma^2}{2\pi f_d\sqrt{1-(f/f_d)^2}} & |f| \leq f_d - \epsilon \\ 0 & \text{else} \end{cases} \tag{3.19}$$

where $\epsilon \in \mathbf{R}^+$ is a small positive real number, which can be taken as multiples of the smallest positive number the computing platform that can handle. Then we solved the numerical optimization problem, for fixed γ, f_d and Q,

$$w_x \;\; = \;\; \arg\min \|S(f;\epsilon) - |G_\gamma(j2\pi f)|^2\|. \tag{3.20}$$

The result of this numerical optimization (3.20) gives the minimizer of the norm of the distance between the modified theoretical spectral density and the theoretical fading filter spectrum. In Table 3.1 ratio of w_x/w_d with respect to various filter orders and desired peak at $w_x = w_d$ is tabulated. Theoretical and approximate spectral density, where the approximate spectral density is for the output of the filter $G_3(s)$, are provided in Figure 3.3.

For the transfer functions provided in the s-domain, we can use the *bilinear transform* to get $G_\gamma(z)$ with an ARMA(γ,γ) model, or *impulse invariance method* to get a $G_\gamma(z)$ with an AR(γ) model (all pole filter), where

$$G_\gamma(z) = \frac{\sum_{k=0}^{\gamma} g_k^M z^{-k}}{1 - \sum_{k=1}^{\gamma} g_k^A z^{-k}} \tag{3.21}$$

with $\{g_k^A\}_{k=1}^{\gamma}, \{g_k^M\}_{k=0}^{\gamma}$ are the auto-regressive and moving-average filter taps, of the ARMA(γ,γ) model, respectively. The generated Rayleigh fading process has an auto-

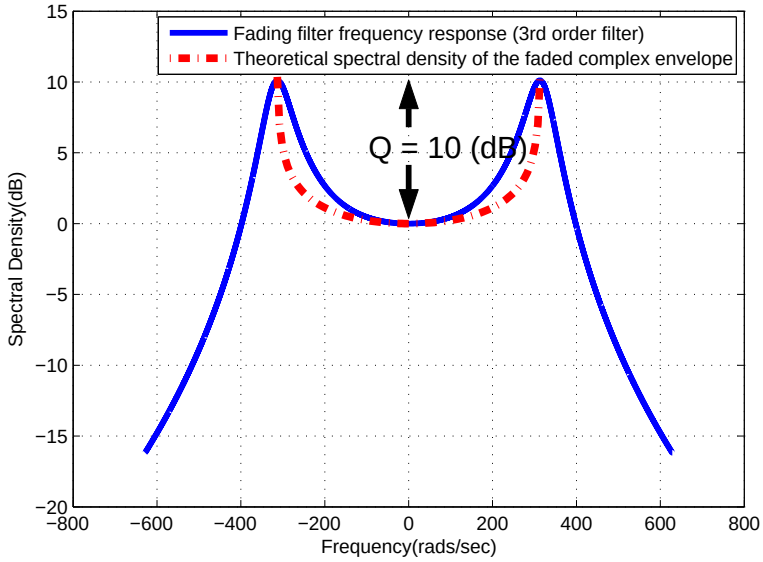

Figure 3.3. Theoretical and approximate spectral density (for the filter $G_3(s)$)

Table 3.1. Ratio of w_x/w_d tabulated with respect to various filter orders and desired peak (dB) at $w_x = w_d$

Filter Order	*Desired Peak (dB) at* $w = w_x$		
γ	*10*	*15*	*20*
2	1.0200	1.0055	1.0025
3	1.0152	1.0060	1.0017
4	1.0668	1.0401	1.0247
5	1.0668	1.0413	1.0228

correlation function, $R_{xx}[n]$, which can be found by directly using Wiener-Khinchine theorem (Proakis and Manolakis 2007). That is,

$$R_{xx}[n] = \sigma^2 g[n] * g[-n] \tag{3.22}$$

where σ^2 is the variance of the complex zero-mean white Gaussian noise, and $g[n] = \mathcal{Z}^{-1}(G_\gamma(z))$ is the discrete time filter impulse response and as given as the inverse $\mathcal{Z}$-transform of the transfer function $G_\gamma(z)$.

3.2.4. Quantized Filter Application of Proposed Filter Design

Hardware implementations can require filters to use minimum power, generate minimum heat, and avoid computational overload in their processors. Meeting these constraints often requires the use of quantized filters.

Because of finite signal lengths and the finite memory of computer processors, only a finite set of quantized sequences is possible. Sampling and quantization round or truncate signal values within the finite set of possibilities. Quantized samples are represented by a group (*word*) of zeros and ones (*bits*) that can be processed digitally. The finer the quantization, the larger the number of bits in the sample word.

Like sampling, improper quantization leads to loss of information. Unlike sampling, however, no matter how fine the quantization, the effects are irreversible, since word lengths must be finite. Finite word lengths appear as nonlinear effects (such as overflow and limit cycles) and can make systematic treatment of quantization extremely difficult. Quantization noise can be described in statistical terms, and is usually considered only in the final stages of design.

Before the application of quantized filtering it is necessary to understand fixed point arithmetic. Hence, we provide a short overview about fundamental concepts of fixed point arithmetic.

3.2.4.1. Fixed Point Arithmetic

One can specify how numbers are quantized using fixed-point arithmetic. The two most important parameters are:

- Word length *w* in bits

- Fraction length *f* in bits

The fraction length is the number of bits between the binary point and the least-significant bit.

Where you place the binary point determines how fixed-point numbers are interpreted. For example, for a signed (twos complement) fixed-point number, 10.110 represents $-2 + 2^{-1} + 2^{-2} = -1.25$.

A fixed-point quantization scheme determines the dynamic range of the numbers that are used. Numbers outside this range are always mapped to fixed-point numbers within the range when you quantize them. The *precision* is the distance between successive numbers occurring within the dynamic range in a fixed-point representation.

- For a signed fixed-point number with word length w and fraction length f, the dynamic range is from -2^{w-f-1} to $2^{w-f-1} - 2^{-f}$.
- For an unsigned fixed-point number with word length w and fraction length f, the dynamic range is from 0 to $2^{w-f} - 2^{-f}$.
- In either case the precision is 2^{-f}.

When you quantize a number outside of the dynamic range, *overflows* occur. Overflows are more frequent with fixed-point quantization than with floating-point quantization, because the dynamic range is less for equivalent word lengths. Overflows can occur when you create a fixed-point quantized filter from an arbitrary floating-point design. You can either *normalize* your coefficients (and introduce a corresponding scaling factor for filtering) to avoid overflows, or else *saturate* or *wrap*.

3.2.4.2. Quantized Filter Application Results

In this section, we implement our proposed ARMA(3,3) filter as a fixed-point filter. Both fixed point filters and single precision floating point filters are referred to as *quantized filters*. We use MATLAB Filter Design Toolbox to implement the fixed-point scheme. After determining the filter coefficients of our proposed filter, we construct the discrete time filter object *hd* by evaluating the MATLAB script *hd = dfilt.df2(b,a)*. This script returns a discrete-time, direct-form II filter object *hd*, with numerator coefficients *b* and denominator coefficients *a*. To create the fixed-point direct-form II filter, we must

change the *Arithmetic* property setting for *hd* to fixed-point arithmetic by evaluating this MATLAB script *set(hd,'Arithmetic','fixed')*.

There are several parameters for fixed-point filter. First we concentrate on the coefficient word length and fraction length (scaling). Then we compare the magnitude responses for both the quantized filter and the corresponding reference filter. To determine the number of bits being used in the fixed-point filter *hd*, one must look at the *CoeffWordLength* property value. To look at the coefficient word length, MATLAB script *get(hd,'CoeffWordLength')* must be evaluated and to look at the fraction length, MATLAB script *get(hd,'NumFracLength')* must be evaluated. If *CoeffWordLength* value is 16 and *NumFracLength* value is 21, this means that hd uses 16 bits to represent the coefficients, and the least significant bit (LSB) is weighted by 2^{-21}. 16 bits is the default coefficient word length the filter uses for coefficients, but the 2^{-21} weight has been computed automatically to represent the coefficients with the best possible precision, given the coefficient word length value.

In the Figure 3.4, the magnitude responses for the various versions of fixed-point filter hd are plotted. So we can compare the effects of changing the coefficient word length. Magnitude responses of all versions of the fixed-point filter, except 10 bits version, and magnitude response of the reference filter are nearly the same. Peak value of the magnitude response of the 10 bits version is 2-3 dB less than the other versions of the fixed-point filter and the reference filter. But comparison of the magnitude responses does not ensure the performance of the fixed-point filter during filtering.

To evaluate the accuracy of the fixed-point filter, we filter complex white Gaussian noise with both filters to generate the Rayleigh fading sequence. When evaluating the accuracy of fixed-point filtering, three quantities for comparing between the quantized filter and the reference filter must be considered:

- The ideal filtered output: This is the goal. It is computed by using the reference coefficients and double-precision floating-point arithmetic.

- The best-you-can-hope-for filtered output: This is the best one can hope to achieve. It is computed by using the quantized coefficients and double-precision floating-point arithmetic.

- The filtered output can actually be attained with the quantized filter: This is the

output computed by using the quantized coefficients and fixed-point arithmetic.

To represent the complex white Gaussian noise as a fixed-point object, we evaluate the MATLAB script, *xin = fi(x,true,'WordLength','FractionLength')*. We can compute the actually attained filtered output by filtering this fixed-point object through the quantized filter and we can compute the best-you-can-hope-for filtered output by casting the fixed-point filter to double-precision and filtering this fixed-point object with double-precision floating-point arithmetic. In this case we must also cast the input data *xin* to double format to use it with the double-precision filter. We can compare these two outputs by taking the norm of the difference of them. If we select the 'WordLength' of the fixed-point input equals to 16 bits, 'FractionLength' of the input equals to 21 bit, and filter 1000 samples through fixed-point filter with 16-bit quantized coefficients, in two aforementioned different case then the norm of the difference of the two outputs equals to 1.5649×10^{-4}. This means that the accumulator is introducing neglible quantization error. For completeness, we must compare the ideal filtered output to the actually attained filtered output. If we take the norm of the difference of the ideal filtered output and the actually attained output, when the 'WordLength' of the fixed-point input equals to 16 bits and the 'FractionLength' of the input equals to 21 bits, this norm equals to 0.2637. When the 'WordLength' of the fixed-point input equals to 14 bits and the 'FractionLength' of the input equals to 18 bits, then the error equals to 0.7964. But if we select the 'WordLength' of the fixed-point input equals to 10 bits and the 'FractionLength' of the input equals to 13 bits, and we also select the coefficient wordlength equals to 10 bits, then the norm of the difference of the attained and ideal filtered outputs equals to 1.5083. In this case, 10-bit quantized coeffients is not enough the represent the filter output accurately. The error in 16 bits case is rather small, but error in 14 bits case and especially in 10 bits case are bigger than 16 bits case. By implementing 10-bits fixed-point filter, we can not achieve enough accuracy.

In Figure 3.5 actually attained outputs of 10 bits, 14 bits,16 bits and ideal filtered output are provided for comparison. Also in Figure 3.6, Figure 3.7 and Figure 3.8, the Rayleigh faded outputs of the 10-bits case and 24-bits case are given respectively.

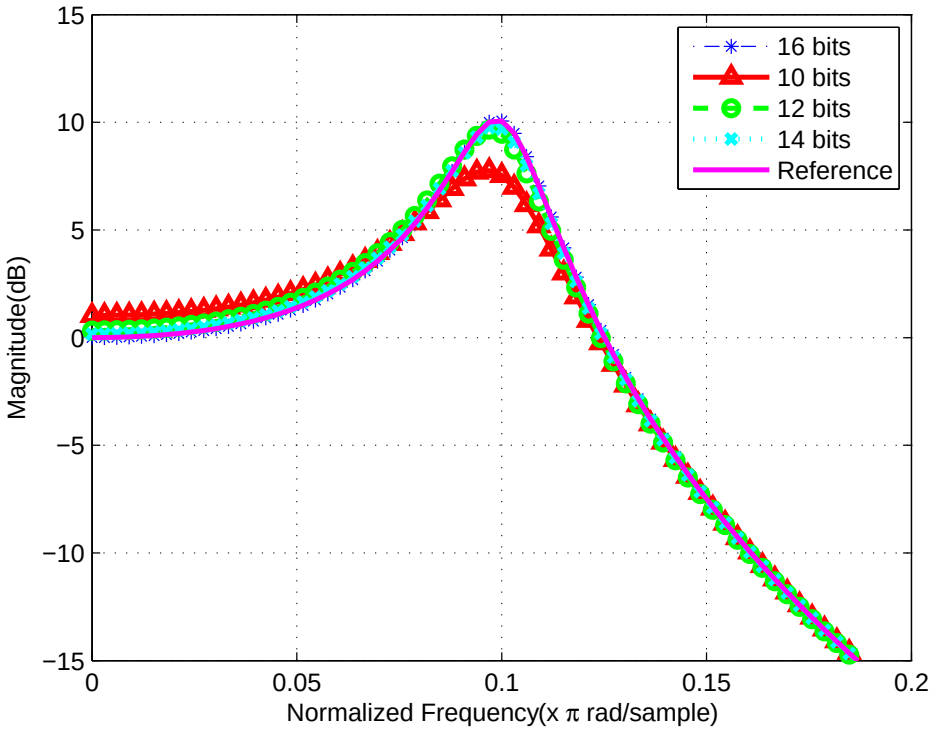

Figure 3.4. Magnitude responses for the various versions of quantized filter and the reference filter

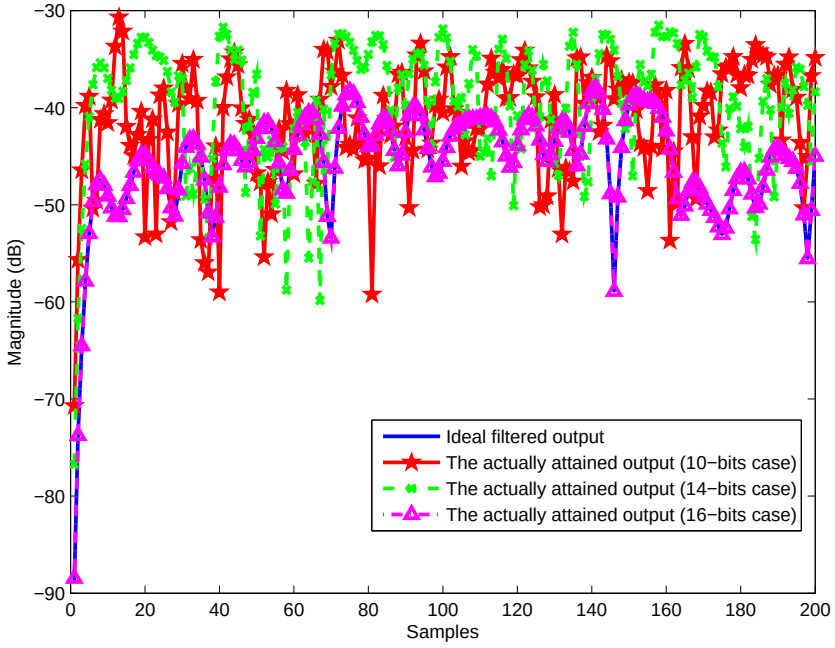

Figure 3.5. The actually attained outputs of 10,14,16 bits case and the ideal output

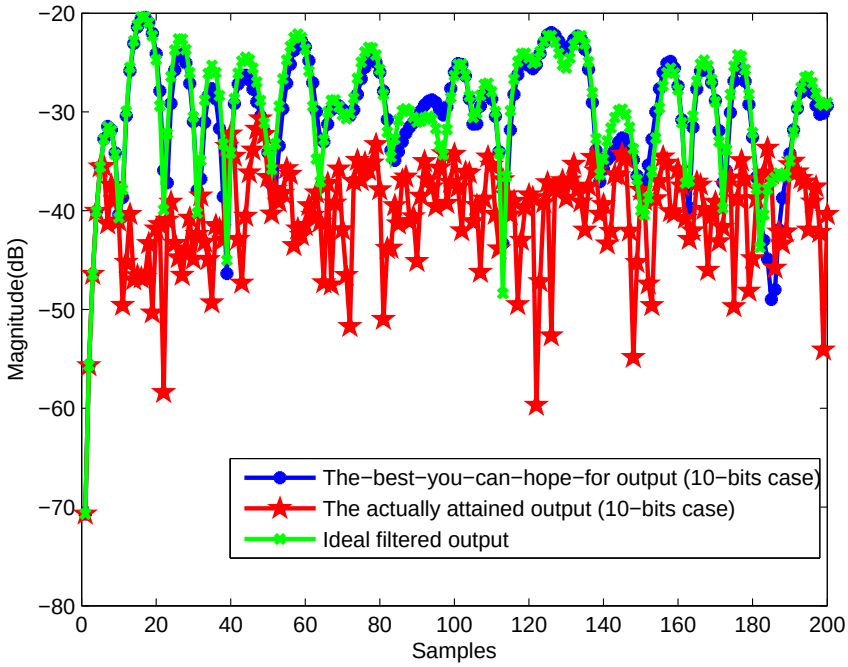

Figure 3.6. The filtered outputs for 10-bits case

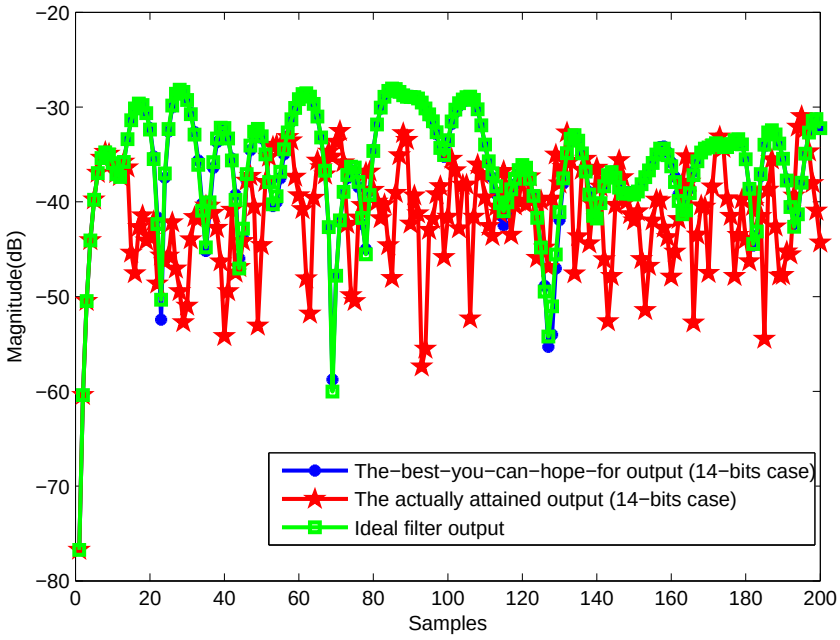

Figure 3.7. The filtered outputs for 14-bits case

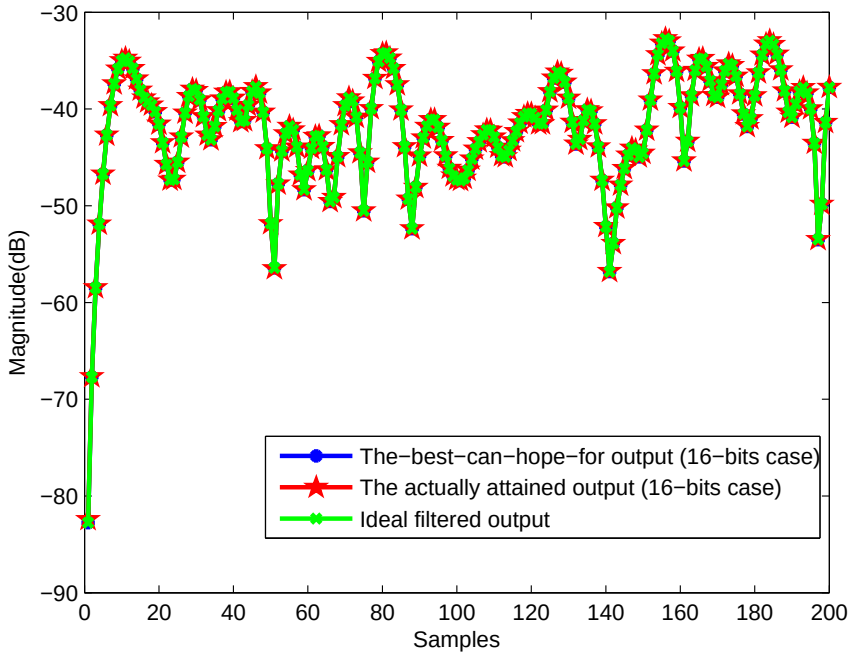

Figure 3.8. The filtered outputs for 16-bits case

3.3. Performance and Complexity Evaluation

In this section, we evaluate the suitability of our proposed filter design technique for producing high-quality Rayleigh fading sequence. Comparisons of our proposed method provided in Section 3 are made to a WSS-improved Jakes' model (Zheng and Xiao 2002), AR fading filter approximation (Baddour and Beaulieu 2005), and to the IDFT technique (Young and Beaulieu 2000) which was shown in to be the most efficient and highest quality method among different Rayleigh fading generator design methods. First, the quantitative measures that are used for this comparison are described.

3.3.1. Quantitative Measures

Quantitative quality measures for generated random sequences have been proposed in (Young and Beaulieu 2003). Two quality measures have been defined as follows. The first measure, called the *mean basis power margin*, is given by

$$\mathcal{G}_{mean} = \frac{1}{\sigma_X^2 L} trace\{C_X C_{\hat{X}}^{-1} C_X\} \tag{3.23}$$

and the second measure, the *maximum basis power margin*, is defined as

$$\mathcal{G}_{max} = \frac{1}{\sigma_X^2} max\{diag\{C_X C_{\hat{X}}^{-1} C_X\}\} \tag{3.24}$$

In (3.23) and (3.24), σ_X^2 is the variance of the reference(ideal) distribution,$C_{\hat{X}}$ is the $L \times L$ covariance matrix of any length-L subset of adjacent samples produced by the stationary random sequence generator, and C_X represents the desired covariance matrix of L ideally distributed samples.

3.3.2. Performance Comparisons

Before evaluating the quality measures, we demonstrate the BER simulation results for both binary shift keying (BPSK) and quadrature phase shift keying modulation schemes in Rayleigh channel generated by our proposed filter, AR(20) filter, and Jakes' model. All of the results are calculated by using 10^6 channel samples. These results are presented in Figure 3.9 and in Figure 3.10.

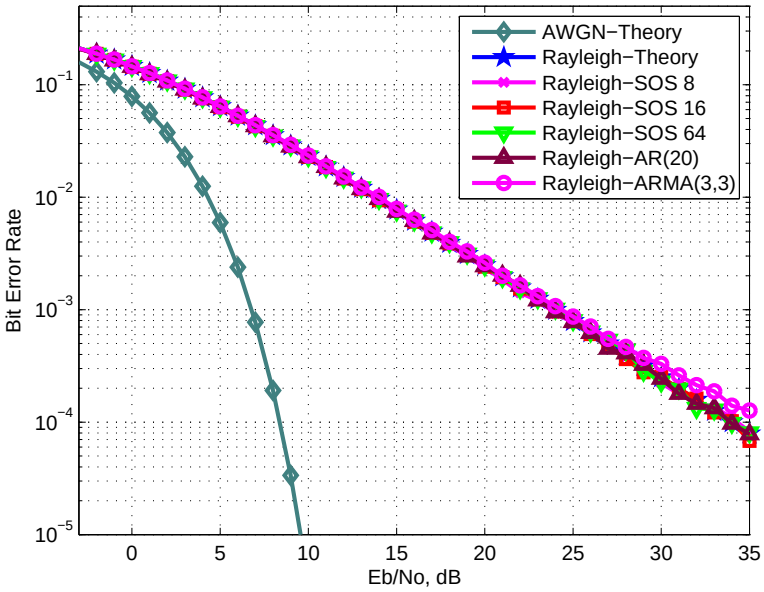

Figure 3.9. BER for BPSK modulation in Rayleigh channel

As seen on the Figure 3.9 and Figure 3.10, BER performances of all Rayleigh fading sequence generators are nearly the same; so we can only compare this generation methods in terms of the quality of the generated autocorrelation sequences and computational complexity.

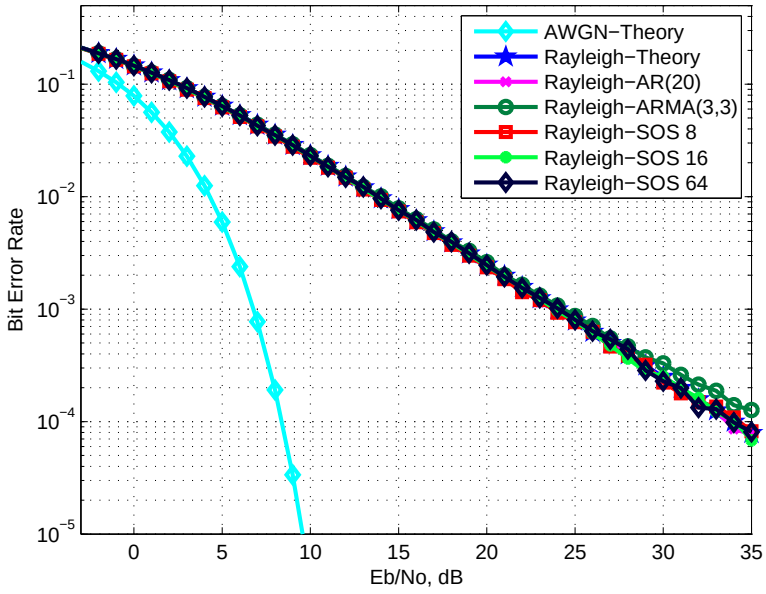

Figure 3.10. BER for QPSK modulation in Rayleigh channel

The quality measure comparison results, which are presented in Table 3.2, compare the quality of the real part of the simulator outputs. Similar results were achieved for the imaginary sequences and these are omitted for brevity. Perfect Rayleigh fading sequence generation method corresponds to 0 dB for both measures. In all cases, the reference autocorrelation function is (2.27) with a normalized maximum Doppler of $f_d \cdot T_s = 0.05$ where $1/T_s$ denotes the sample rate. An autocorrelation sequence length of 200 was considered for evaluation of all theoretical results. For the empirical results, time average correlations were calculated based on 2^{20} generated samples. The computed quality measures were then averaged over 50 independent simulation trials. Plots of the empirical autocorrelation functions of the AR model and our proposed Rayleigh fading generator via AR models are shown in Figure 3.11 and the plots of the IDFT method and our proposed filter generator via ARMA models are shown in Figure 3.12. The results show that the IDFT method generally provides closer the highest quality Rayleigh samples. The AR model provides a more precise match to the desired autocorrelation function as the order of the model used increases. But our proposed filter design method provides same accuracy with much lower order models. Our ARMA(3,3) generator has a significant advantage over AR(20) generator. Similar accuracy can be achieved by the WSS sinusoidal generator when a large number of sinusoidal oscillators are used.

Table 3.2. Quality measures for the IDFT, our proposed filter design via AR and ARMA, AR filtering and sum of sinusoids methods

Rayleigh Fading Random Sequence Generators		Theoretical(dB)		Empirical(dB)	
		$\mathcal{G}_{mean}$	$\mathcal{G}_{max}$	$\mathcal{G}_{mean}$	$\mathcal{G}_{max}$
IDFT Method		0.00076	0.00081	0.0035	0.0037
Proposed Filter Design	ARMA(2,2)	2.5066	2.5505	2.5068	2.5514
	AR(2)	2.6707	2.7247	2.6768	2.7313
	ARMA(3,3)	1.9777	1.9962	1.9775	1.9979
	AR(3)	2.0924	2.1173	2.1447	2.1727
AR Filtering	AR(20)	2.7	2.9	2.6	2.9
	AR(50)	0.29	0.43	0.26	0.40
	AR(100)	0.13	0.28	0.11	0.26
Sum of Sinusoids	8 Sinusoids	N/A	N/A	36.223	37.730
	16 Sinusoids	N/A	N/A	4.0264	6.4140
	64 Sinusoids	N/A	N/A	0.0211	0.0370
	128 Sinusoids	N/A	N/A	0.0027	0.0049

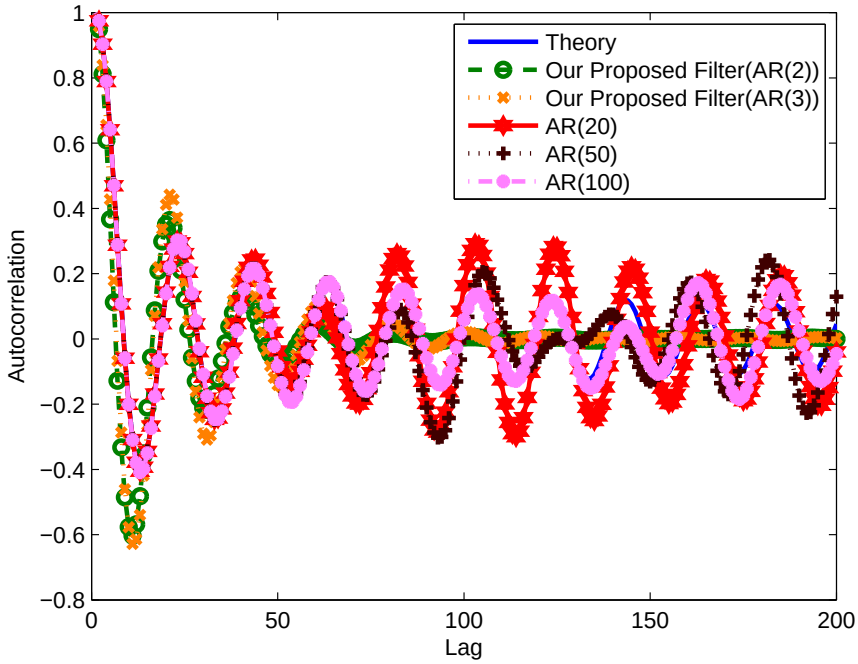

Figure 3.11. The empirical autocorrelations for AR method and proposed model

Table 3.3. Computational Complexity comparison

Simulator Design Technique		Number of Real Multiplications
IDFT Method		44×10^6
Proposed Filter Design	ARMA(2,2)	8×10^6
	AR(2)	2×10^6
	ARMA(3,3)	12×10^6
	AR(3)	6×10^6
AR Filtering	AR(20)	42×10^6
	AR(50)	105×10^6
	AR(100)	210×10^6
Sum of Sinusoids	8 Sinusoids	178×10^6
	16 Sinusoids	356×10^6
	64 Sinusoids	1424×10^6
	128 Sinusoids	2848×10^6

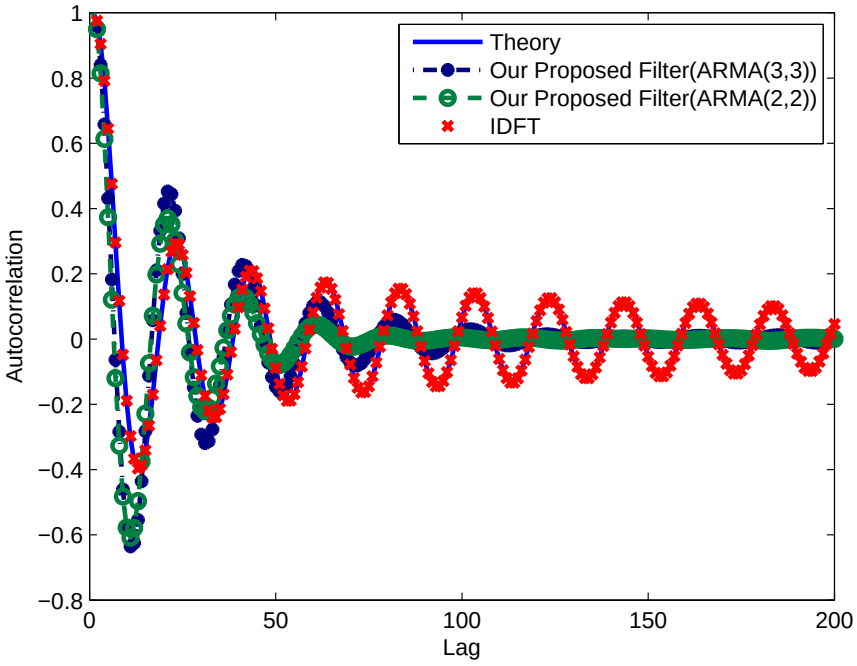

Figure 3.12. The empirical autocorrelations for IDFT method and proposed model

The main advantage of our low complexity Rayleigh fading generator is that the samples of the fading sequence can be generated as they are required while achieving the lowest complexity of all the Rayleigh fading generators mentioned. The computational efficiency of the IDFT method brings a cost in storage requirements as all samples are generated using a single IFFT. Our proposed fading generator and the all other generators don't have such a limitation. As provided in Table 3.3, to generate 2^{20} samples, IDFT method requires 44×10^6 real multiplications, our proposed filter design technique via ARMA(3,3) model requires 12×10^6 real multiplications, AR(20) model requires 42×10^6 multiplications and the improved Jakes' model with 16 sinusoids requires 356×10^6 multiplications.

CHAPTER 4

PATH LOSS AND SHADOWING PREDICTIONS

To predict the path loss and shadowing is very important for wireless channel modeling and wireless communication system design. In this chapter, path loss and shadowing predictions will be made by using a site-specific radio propagation software called Wireless InSite. In the first part, some theoretical information about path loss is given with an experiment done in Wireless InSite, where the path loss is calculated in a propagation scenario including a transmitter, a receiver route, and a concrete barrier. The aim of this experiment is to predict the power loss in a shadowed region. Then we provide theoretical information about shadowing.

4.1. Path Loss

Path loss refers to the attenuation in the transmitted signal while propagating from the transmitter to the receiver. Path loss is caused by dissipation of the radiated power as well as effects of the propagation channel such as absorption due to moisture. Typical path loss models assume a distance dependence attenuation, i.e., the received power is a function of the distance between the transmitter and the receiver. Significant variations in the path loss are observed over distances of several hundred to thousand wavelengths.

The simplest path loss model corresponds to propagation in free space, i.e., line-of-sight (LOS) link between the transmitter and receiver. Under this model, the received signal power is given as

$$P_R = P_T G_T G_R \frac{\lambda^2}{4\pi d^2} \tag{4.1}$$

where P_T is the transmitted power, G_T and G_R are the transmit and receive antennas gains, respectively, λ is the wavelength of the transmitted carrier, and d is the distance between the transmitter and the receiver. Thus, the received power decreases with a factor of distance-squared under free space propagation. We also observe the path loss dependency on the carrier wavelength. Shorter the wavelength or equivalently higher the transmitter frequency, higher the path loss.

The free space path loss model cannot capture all the propagation scenarios encountered in the real world. Therefore, several different models such as Okumura, Hata, Walfish-Ikegami, etc., have been proposed to model path loss in different propagation environments such as urban, rural, and indoor areas.

4.1.1. Shadowing Loss Prediction Experiment

In this section, we investigate the effect of a barrier on the received power, which completely blocks the line of sight. Therefore there exists a shadowed region behind the barrier. We make path loss prediction by using Wireless InSite. Our experimental setup in Figure 4.1 includes a transmitter with a height of 30 m, a receiver route with a length of 1 km, where the distance between the receivers is 5 m, and a barrier which is 20 m height. All of the antennas used in this experiment are half-wave dipole antenna and the transmitted signal waveform is sinusoid with a carrier frequency equals to 900.5 Mhz, so the wavelength is 0.3331 m.

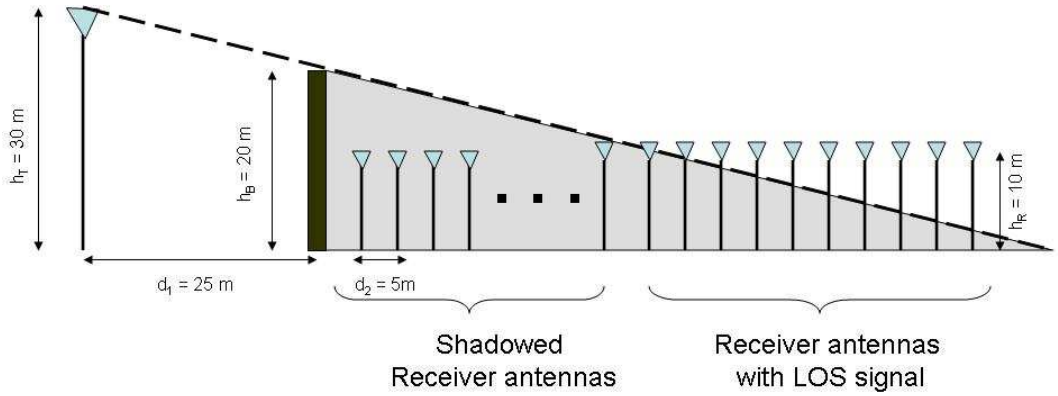

Figure 4.1. Experimental setup to predict the shadowing loss

Figure 4.2 shows the plots of the predicted results. As seen on the figures the shadow region covers the area bounded with distances of 0 m - 70 meters. In this region the fluctuations of the received signal strength are caused from diffraction (for more information refer to (Saunders 1999)). If we distract the theoretical path loss from the total loss measured in shadowed region then we can achieve the shadowing loss. After the distance of 70 m the values that we predict are approximately equal to the theoretical values and the predicted values obtained by the experiment done without barrier.

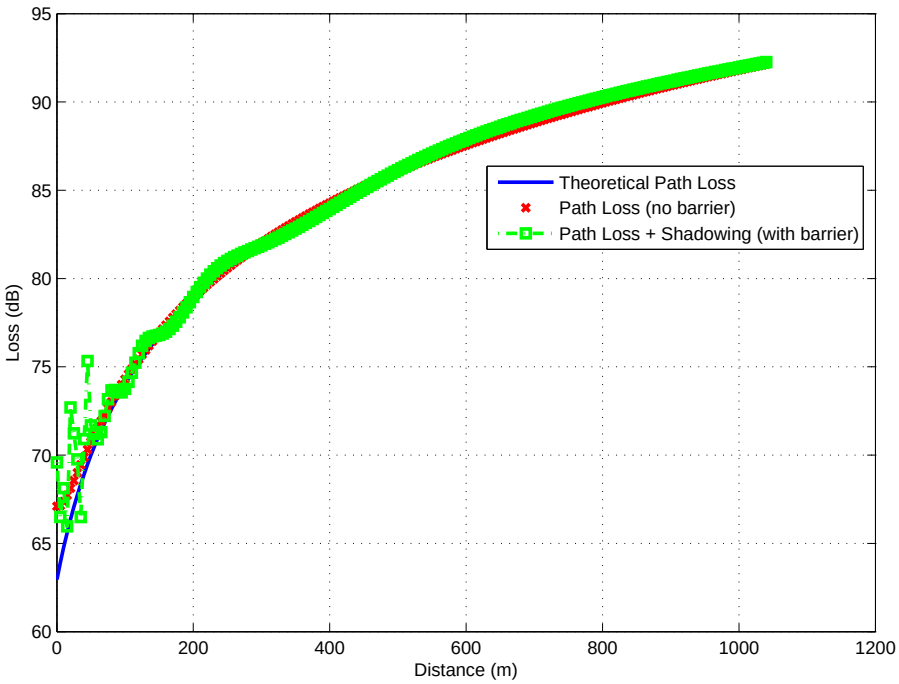

Figure 4.2. Predicted path loss and shadowing values

4.2. Shadowing

The presence of obstacles such as buildings and trees results in random variations of the received power at a given distance. Measurements have been made under several different conditions and statistical variations have been observed. Different values of the received signal power were measured for a fixed frequency and distance. Thus for a given fixed distance, frequency and transmission power, the received signal power is not deterministic, but varies due to the objects in and around the signal path. These stochastic, location dependent variations are called *shadowing* and were denoted in Equation 1.1 by $a_{SH}(t)$. But these stochastic variations are constant in time, as long as the receiver and its complete environment do not move. Shadowing reflects the differences in the measured received power with relation to the theoretical value calculated by path loss formulas. However averaging over many received power values for the same distance yields the exact value given by path loss.

The objects causing these variations are of very large dimensions that a receiver moving along a line at constant distance from the transmitter will take several hundreds of milliseconds (ms) to move an area with different characteristics. As a result, path loss

and shadowing are often called large scale effects. Large scale effects play an important role in the system design at the network level. For instance, the cell coverage area, outage, and handoffs are influenced by these effects.

4.2.1. Shadowing Model

Experimental results show that the shadow fading can be fairly accurately modeled as a log-normal random variable (Okumura, et al. 1968), (Reudink 1972), (Black and Reudink 1972), (Ibrahim and Parsons 1983), (Gudmundson 1991). This hypothesis has been verified with χ^2 and Kolmogorov-Smirnov test and found to be valid with high confidence intervals. The theoretical basis to the log-normal distribution is that in an environment different signals suffer random reflections and diffractions as they traverse the propagation medium. If the total loss is expressed in dB then the extra loss due to the shadowing in each path corresponds to subtracting a random loss from the path loss value. Since the different propagation paths are independent, the sum of all the dB losses for a large number of propagation paths converges to a normally distributed random variable (central limit theorem). In natural units, that becomes a log-normal distribution.

The pdf of the shadowing is given by:

$$p(a_{SH}) = \frac{1}{\sigma_{SH}\sqrt{2\pi}} \exp\left(-\frac{a_{SH}^2}{2\sigma_{SH}^2}\right) \tag{4.2}$$

where σ_{SH} is the standard deviation of a_{SH} and all variables are expressed in dB.

The value of the variation due to the shadowing is then added to the path loss value to obtain the variations. This value is determined by

$$a[dB] = 10 \cdot \log \frac{P_0}{P_t} = a_{PL}[dB] + a_{SH}[dB] \tag{4.3}$$

where P_0 is the received power and P_t is the transmitted power.

4.2.2. Shadowing Correlation

The autocorrelation of the shadowing process in space also needs to be modeled, since values at close locations are expected to be correlated. The spatial correlation is given by the exponential correlation model proposed by (Gudmundson 1991) based upon an approximate fitting of empirical data. According to this model, the spatial correlation

is quantified as

$$R_{SH}(\Delta x) = \sigma_{SH}^2 \exp(-|\Delta x|/d_c) \tag{4.4}$$

where Δx is the spatial separation between points at which the correlation is measured and d_c is the spatial de-correlation distance. Typically, the shadowing de-correlation distance d_c ranges from 10-50 m. It must be noted that though theoretical results prevent an exponential correlation model for shadowing, it is still widely used because of providing a reasonably good fit to experimental data (Mandayam, et al. 1996).

When the Rx is mobile, these spatial correlation translates into time correlation. Therefore, the shadowing behaves as a correlated, time-varying process. The time auto-correlation can be obtained from 4.4 by substituting $\Delta x = vt$, where v is the Rx speed and t is the time variable.

Large scale effects play an important role in the system design at the network level. For example, the cell coverage area, outage, and handoffs are influenced by these effects. The above discussion suggests that shadowing variations become significant when the receiver moves over distances greater than several tens of the carrier wavelength. As a result, these effects are often called large scale effects. On the other hand, small scale fading caused by multipath propagation, determines the link level performance in terms of the bit error rate (BER), average fade durations, etc.

CHAPTER 5

SIMULATION OF SPATIAL SHADOWING PROCESS

In this chapter, we simulate spatial shadowing process by using the 1-D simulation model proposed in (Pätzold and Nguyen 2004). The simulation model is derived from a non-realizable reference model by replacing the underlying spatial shadowing process by a finite sum of sinusoids with constant gains, constant spatial frequencies, and random phases. Constant gains and constant spatial frequencies are the model parameters. Two parameter computation methods are discussed enabling the fitting of the simulation model to the reference model with respect to the PDF of the received signal strength as well as to a given spatial autocorrelation function. Theoretically, this autocorrelation function is well-known decaying exponential function which is proposed in (Gudmundson 1991). We also predict an autocorrelation function by using a site-specific radio propagation software named Wireless InSite. We used both predicted and theoretical autocorrelation functions to determine the model parameters.

5.1. Reference Model for Shadowing

The effect of shadowing is generally modeled as a log-normal process $\lambda(t)$, which can be expressed as

$$\lambda(t) = 10^{[\sigma_L \nu(t) + m_L]/20} \tag{5.1}$$

where $\nu(t)$ is a real valued Gaussian process with unit variance. The parameters σ_L and m_L in 5.1 are called the shadow standard deviation and the area mean, respectively. The area mean m_L is obtained by averaging the received signal strength over an area that is large enough to average over the shadowing effects (Stüber 2001). The value of m_L is determined by the path loss between the BS and the MS. The value of σ_L increases slightly with the antenna heights and the environment. The shadow standard deviation σ_L is usually in the range from 5 to 12 dB at 900 MHz (Okumura, et al. 1968), (Reudink 1972), (Black and Reudink 1972), (Ibrahim and Parsons 1983), (Gudmundson 1991) where 8 dB is a typical value for macrocellular applications. Let us assume that the MS

starts at the origin $x_0 = 0$ and moves along the x-axis with velocity v. Then, by using the time-distance relationship $t = x/v$ we can express both the log-normal process $\lambda(t)$ and the Gaussian process $\nu(t)$ as a function of the distance x, i.e., $\lambda(x)$ and $\nu(x)$. There as a result of empirical studies, the following spatial autocorrelation function $r_{\nu\nu}(\Delta x)$ of $\nu(x)$ has been proposed in (Gudmundson 1991)

$$r_{\nu\nu}(\Delta x) = e^{-|\Delta x|/D} \tag{5.2}$$

where Δx denotes the spatial separation which measures the distance between two locations and D is called the de-correlation distance, which is an environment dependant real-valued constant.

It is widely accepted that the PDF $p_\lambda(y)$ of $\lambda(x)$ follows the log-normal distribution

$$p_\lambda(y) = \frac{20}{\sqrt{2\pi}\ln 10\sigma_L y} e^{-\frac{(20\log_{10} y - m_L)}{2\sigma_L^2}} \quad y \geq 0. \tag{5.3}$$

The spatial autocorrelation function $r_{\lambda\lambda}(\Delta x)$ of the log-normal process $\lambda(x)$ can be expressed in terms of the spatial autocorrelation function $r_{\nu\nu}(\Delta x)$ as follows (Pätzold and Nguyen 2004)

$$r_{\lambda\lambda}(\Delta x) = e^{2m_0+\sigma_0^2[1+r_{\nu\nu}(\Delta x)]} \tag{5.4}$$

where $\sigma_0 = \sigma_L \ln(10)/20$ and $m_0 = m_L \ln(10)/20$. From the above equation, the mean power of the spatial log-normal process $\lambda(x)$ can easily obtained as $r_{\lambda\lambda}(0) = e^{2m_0+\sigma_0^2}$. A good approximation of $\tilde{r}_{\lambda\lambda}(\Delta x)$ can be given by (5.4), if we replace there $r_{\nu\nu}(\Delta x)$ by $r_{\nu\nu}(\Delta x)$, i.e.,

$$\tilde{r}_{\lambda\lambda}(\Delta x) = e^{2m_0+\sigma_0^2[1+\tilde{r}_{\nu\nu}(\Delta x)]} \tag{5.5}$$

where $\sigma_0 = \sigma_L \ln(10)/20$ and $m_0 = m_L \ln(10)/20$ as in 5.4.

5.2. The Simulation Model for Shadowing

A stochastic continuous-time simulation model for a log-normal process $\lambda(t)$ is obtained by replacing the Gaussian process $\nu(t)$ in (5.1) by the following sum of N sinusoids

$$\tilde{v}(t) = \sum_{n=1}^{N} c_n \cos(2\pi f_n t + \Theta_n). \tag{5.6}$$

In this equation, the gains c_n and the frequencies f_n are non-zero real-valued constant quantities and the phases Θ_n are independent, identically distributed (iid) random variables, which are uniformly distributed over the interval $(0, 2\pi]$. Therefore, $\tilde{\nu}(t)$ represents a stochastic process, which is first-order stationary and ergodic (Pätzold 2003). The corresponding stochastic spatial process $\tilde{\nu}(x)$ is obtained from (5.6) by applying the time-distance transformation of $t \mapsto x/v = x/(\lambda_c f_{max})$, where λ_c is the wavelength of the carrier frequency and f_{max} denotes the maximum Doppler frequency. Hence, we can express the resulting spatial process $\tilde{\nu}(x)$ as

$$\tilde{\nu}(x) = \sum_{n=1}^{N} c_n \cos(2\pi\alpha_n x + \Theta_n) \tag{5.7}$$

where $\alpha_n = f_n/(\lambda_c f_{max})$ are called the spatial frequencies. By analogy to 5.1, a stochastic simulation model for a spatial log-normal process is then obtained as

$$\tilde{\lambda}(x) = 10^{[\sigma_L \tilde{\nu}(x) + m_L]/20}. \tag{5.8}$$

The structure of the simulation model for spatial shadowing process is shown in Figure 5.1.

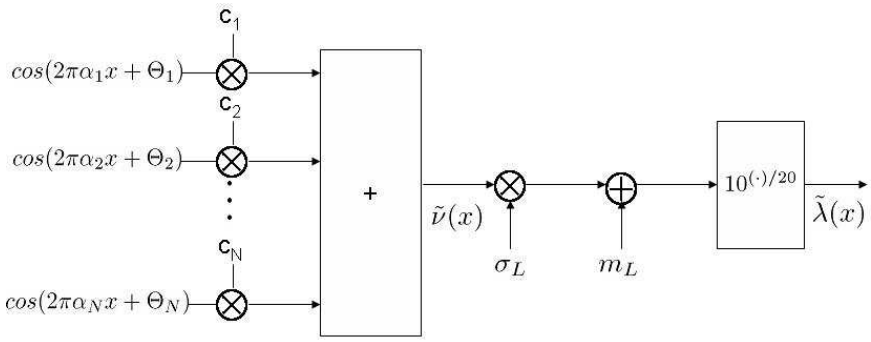

Figure 5.1. Structure of the spatial shadowing simulator

5.2.1. Statistics of the Simulation Model

Since the gains c_n and the spatial frequencies α_n are constant and the phases Θ_n are iid uniformly distributed random variables then it follows from 5.7 that the expected value of $\tilde{\nu}(x)$ equals $E[\tilde{\nu}(x)] = 0$. The variance can be expressed also as $Var\{\tilde{\nu}(x)\} = \sum_{n=1}^{N} c_n^2/2$. Let us define the gains c_n as $c_n = \sqrt{2/N}$, then the variance of $\tilde{\nu}(x)$ equals

unity and thus it is identical with the variance of $\nu(x)$. The spatial autocorrelation function of $\tilde{\nu}(x)$, defined as $\tilde{r}_{\nu\nu}(\Delta x) = E[\tilde{\nu}(x)\tilde{\nu}(x+\Delta x)]$, is given by

$$\tilde{r}_{\nu\nu}(\Delta x) = \sum_{n=1}^{N} \frac{c_n^2}{2} \cos(2\pi\alpha_n \Delta x). \tag{5.9}$$

Since $\tilde{\nu}(x)$ in 5.7 represents a finite sum of sinusoids with random phases, we can use the results presented in (Bennett 1948) to express the PDF $\tilde{p}_\nu(x)$ of $\tilde{\nu}(x)$

$$\tilde{p}_\nu(x) = 2\int_0^\infty \left[\prod_{n=1}^{N} J_0(2\pi c_n z)\right] \cos(2\pi x z) dz \tag{5.10}$$

where $J_0(\cdot)$ denotes the zeroth order Bessel function of first kind.

Applying the concept of transformation of random variables (Stark and Woods 2002), the PDF $\tilde{p}(y)$ of $\tilde{\lambda}(x)$ can be expressed in terms of the PDF $\tilde{p}_\nu(x)$ of $\tilde{\nu}(x)$ as

$$\tilde{p}_\nu(y) = \frac{20\tilde{p}_\nu\left(\frac{20log_{10}y - m_L}{\sigma_L}\right)}{y\sigma_L \ln 10} \tag{5.11}$$

5.2.2. Parameter Computation Methods

There are two fundamental methods for the computation of the model parameters c_n and α_n. The first one is called the method of equal areas and the second one is known as the L_p-norm method.

5.2.2.1. Method of Equal Areas

This method has been introduced in (Pätzold, et al. 1996) to model the classical Jakes/Clark Doppler spectrum and the Gaussian Doppler spectrum. This method can be applied on the spatial autocorrelation function $r_{\nu\nu}(\Delta x)$ of the reference model described by 5.2. Then, the following closed-form expressions are derived:

$$\alpha_n = \frac{1}{2\pi D} \tan[\frac{\pi(n-0.5)}{2N}] \tag{5.12}$$

$$c_n = \sqrt{2/N} \tag{5.13}$$

where $n = 1, 2, \ldots, N$.

Table 5.1. Model parameters of the reference model

Shadowing area	D	Δx_{max}	σ_L	m_L
Suburban	503.9 m	2500 m	7.5 dB	0
Urban	8.3058 m	40 m	4.3 dB	0

5.2.2.2. L_p-Norm Method (LPNM)

The L_p-norm Method (LPNM) was introduced in (Pätzold, et al. 1998). The application of this method implies the minimization of the L_p-norm given in (5.14) where $r_{\nu\nu}(\Delta x)$ and $\tilde{r}_{\nu\nu}(\Delta x)$ are given by (5.2) and (5.9), respectively.

$$E_{r_{\nu\nu}}^{(p)} = \left[\frac{1}{\Delta x_{max}} \int_0^{\Delta x_{max}} |r_{\nu\nu}(\Delta x) - \tilde{r}_{\nu\nu}(\Delta x)|^p d(\Delta x) \right]^{1/p} \quad p = 1, 2, \ldots \tag{5.14}$$

The quantity Δx_{max} indicates the upper limit of the interval $[0, \Delta x_{max}]$ over which the approximation is of interest. In the simulation model both α_n and c_n are the model parameters which have to be optimized numerically until the L_p-norm $E_{r_{\nu\nu}}^{p}$ in (5.14) reaches a local minimum (Pätzold and Nguyen 2004). The numerical optimization can be performed, by using the Fletcher-Powell algorithm (Fletcher and Powell 1963). The most important advantage of the LPNM is that this powerful procedure enables the fitting of the statistical properties of the channel simulator to real world channels simply by replacing the spatial autocorrelation of the theoretical reference model $r_{\nu\nu}(\Delta x)$ by the measured one in the L_p-norm equation (5.14). In this thesis we use our predicted autocorrelation function in order to fit the statistical properties of the channel simulator.

5.2.3. Application of the Simulation Model

In this section, procedure of (Pätzold and Nguyen 2004) is applied to the design of a spatial shadowing simulator. The parameters used to the describe the reference model are given in Table 5.1. The values of the decorrelation distance D and the shadow standard deviation σ_L given in this table are obtained from signal strength measurements (Gudmundson 1991).

The corresponding spatial simulation models in all figures has been designed by

using $N = 25$ sinusoids. The parameters α_n and c_n have been computed by applying both MEA and the LPNM methods, for the aim of comparison. In the LPNM method p was equal to 2. Figure 5.2 and Figure 5.3 show plots of the spatial autocorrelation functions $\tilde{r}_{\nu\nu(\Delta x)}$ for the urban and suburban areas respectively and Figure 5.4 and Figure 5.5 show plots of the spatial autocorrelation functions $\tilde{r}_{\lambda\lambda(\Delta x)}$ of the log-normal processes for the urban and suburban areas respectively. Also in both figures the reference autocorrelation functions $r_{\nu\nu}(\Delta x)$ and $r_{\lambda\lambda}(\Delta x)$ are plotted for comparative purposes.

One can understand from the figures that the performance of the LPNM is higher than that of the MEA. But the MEA results in a closed form solution whereas the LPNM does not. One can obtain better results from MEA, if the number of sinusoids tends to infinity. Because, at that time the simulation model converges to the reference model. So advantages of the LPNM reduce the higher the number of sinusoids is chosen.

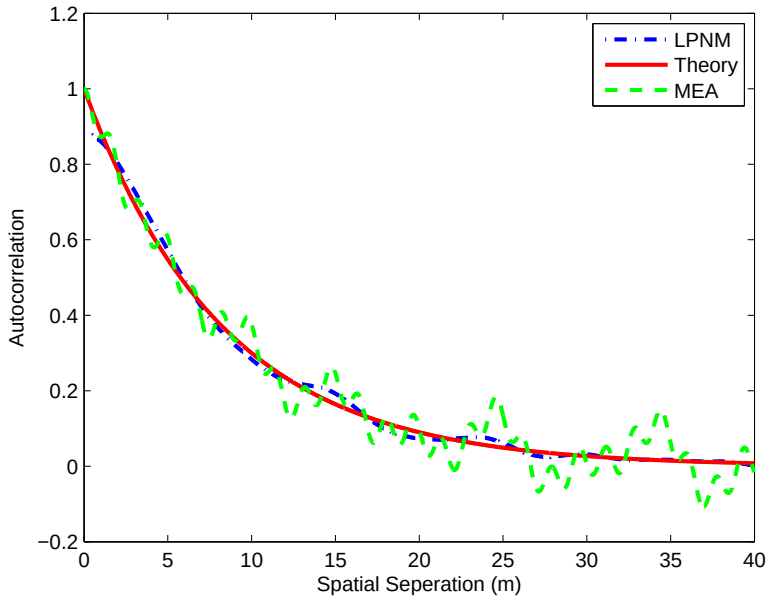

Figure 5.2. Spatial autocorrelation functions $r_{\nu\nu}(\Delta x)$ and $\tilde{r}_{\nu\nu}(\Delta x)$ for the urban area (N = 25)

5.3. Prediction of Autocorrelation of Spatial Shadowing Process

LPNM provides a big advantage for simulating spatial shadowing process by using sum of sinusoids based simulators. Because the model parameters of this method is acquired via numerical optimization and one can fit the spatial shadowing simulator to

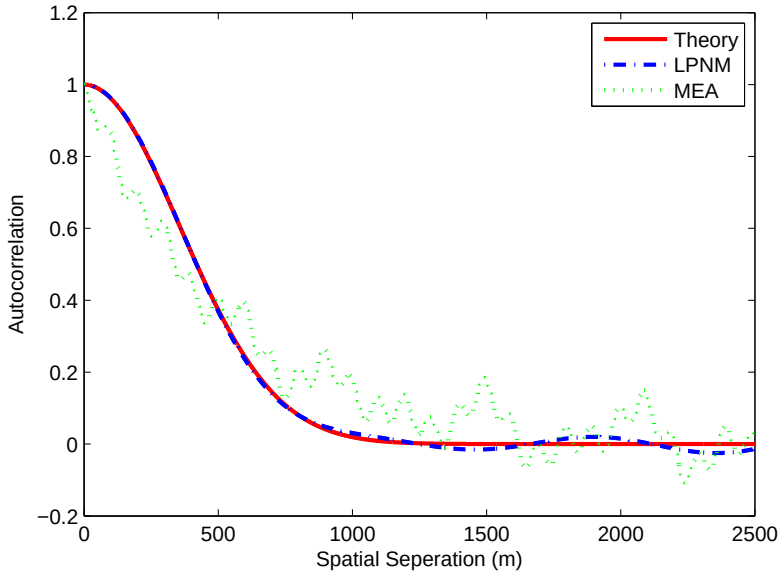

Figure 5.3. Spatial autocorrelation functions $r_{\nu\nu}(\Delta x)$ and $\tilde{r}_{\nu\nu}(\Delta x)$ for the suburban area (N = 25)

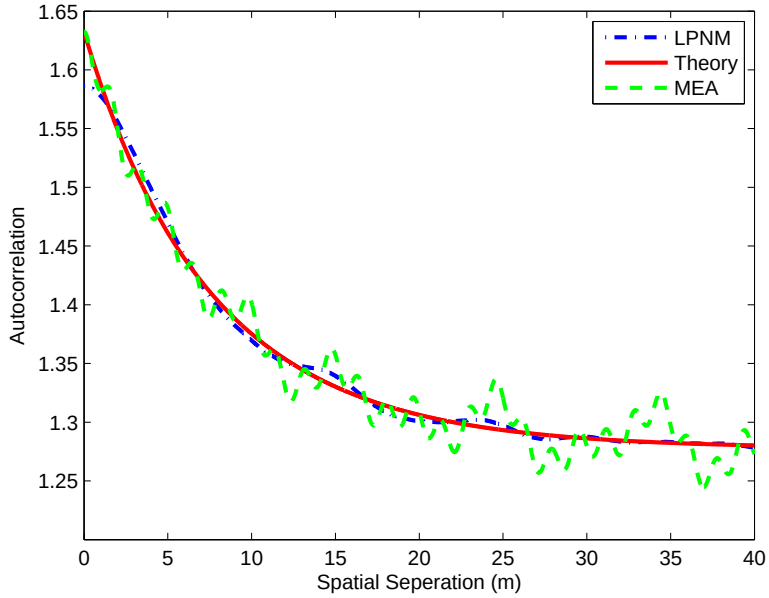

Figure 5.4. Spatial autocorrelation functions $r_{\lambda\lambda}(\Delta x)$ and $\tilde{r}_{\lambda\lambda}(\Delta x)$ for the urban area (N = 25)

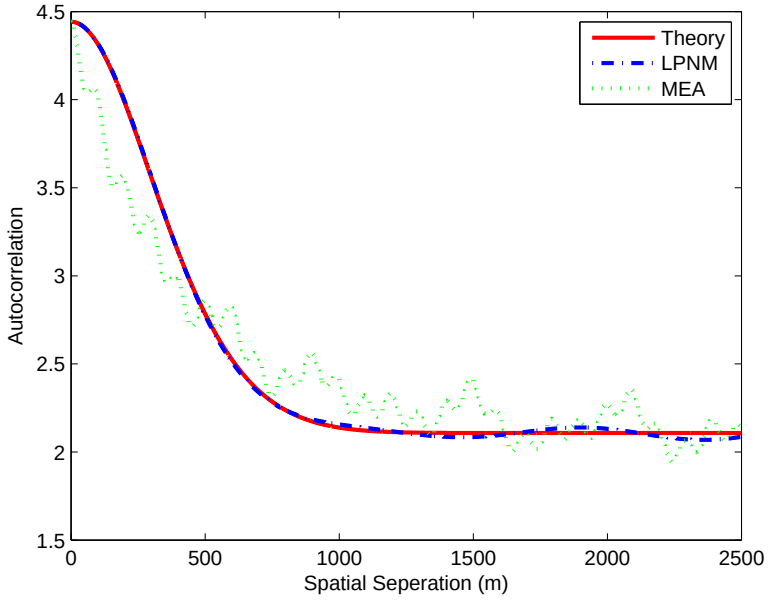

Figure 5.5. Spatial autocorrelation functions $r_{\lambda\lambda}(\Delta x)$ and $\tilde{r}_{\nu\nu}(\Delta x)$ for the suburban area (N = 25)

real world channels by replacing the spatial autocorrelation of the theoretical model by the measured one in the optimization equation (5.14) of simulation model parameters. So we can measure or predict a spatial autocorrelation to fit the channel simulator to real world channels. In this section, we make a urban propagation experiment by using Wireless InSite to obtain spatial autocorrelation of shadowing. Then we use this autocorrelation to determine the model parameters of sum of sinusoids based spatial shadowing simulator which is discussed in the previous section.

5.3.1. Autocorrelation Prediction Experiment

One of the most powerful features of Wireless InSite is the ability to apply state-of the-art models and analysis methods to a wide range of propagation problems. In this experiment we predict received power in an urban area to obtain the shadowing auto-correlation. We use Urban Canyon model to make urban propagation predictions in a microcellular environment in a section of Helsinki, Finland. Without specific knowledge of a particular buildings material parameters, a single material can be used for the entire city such as brick or concrete. For this analysis a uniform building material of concrete is used with a dielectric constant of 5.0. We have also chosen to use the predicted received

power values obtained from non-line-of sight AOB street. For this study, antennas similar to the ones used in Zhangs paper (Zhang 2000) are added. A narrow beam directional antenna is used for transmitters, and monopoles for each receiver point and the transmitted signal waveform is sinusoid with a carrier frequency equals to 900.5 MHz as used in the shadowing prediction experiment in Chapter 4. Our project view showing transmitter and receiver route along AOB street is given in Figure 5.6. In this figure the red line denotes the receiver route while the green point denotes the transmitter.

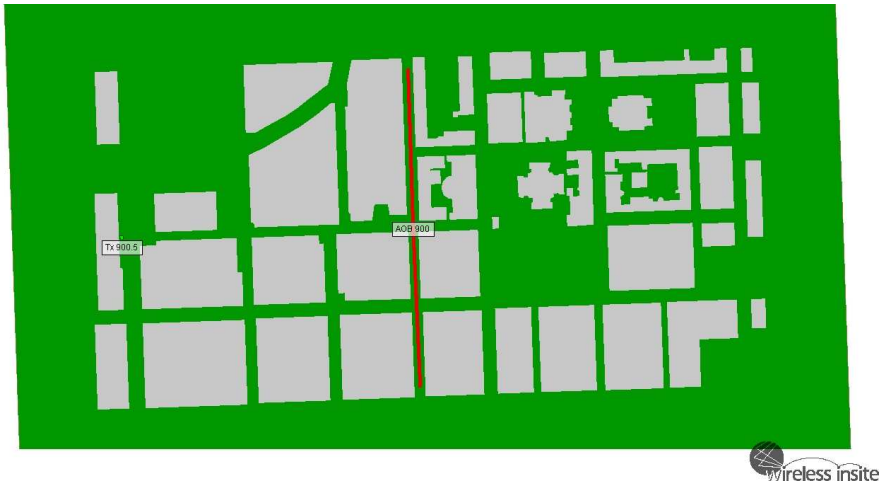

Figure 5.6. Project view showing transmitter and receiver route

Once the received power is calculated, then we should refine the received power data to determine the shadowing autocorrelation. To extract the shadowing characteristics, first the distance dependent path loss is removed from the received power data. Then we average the measured signal as explained in Figure 5.7 over a distance of 2 meters to remove some of the effects of fading.

We calculate the autocorrelation of the spatial shadowing process over a range of lags, using (5.15). The lags correspond to a range of distances where the received power is predicted. In (5.15) x_i denotes the received power value for each lag and ρ_k denotes the autocorrelation value.

$$\begin{aligned} \tilde{x}_i &= x_i - \frac{1}{n}\sum_{i=1}^{n} x_i \\ \rho_k &= \frac{\frac{1}{n-k}\sum_{i=k+1}^{n} \tilde{x}_i \tilde{x}_{i-k}}{\frac{1}{n}\sum_{i=1}^{n} \tilde{x}_i^2} \end{aligned} \tag{5.15}$$

After obtaining of the predicted autocorrelation, this autocorrelation is used to determine the model parameters of sum of sinusoids based spatial shadowing simulation

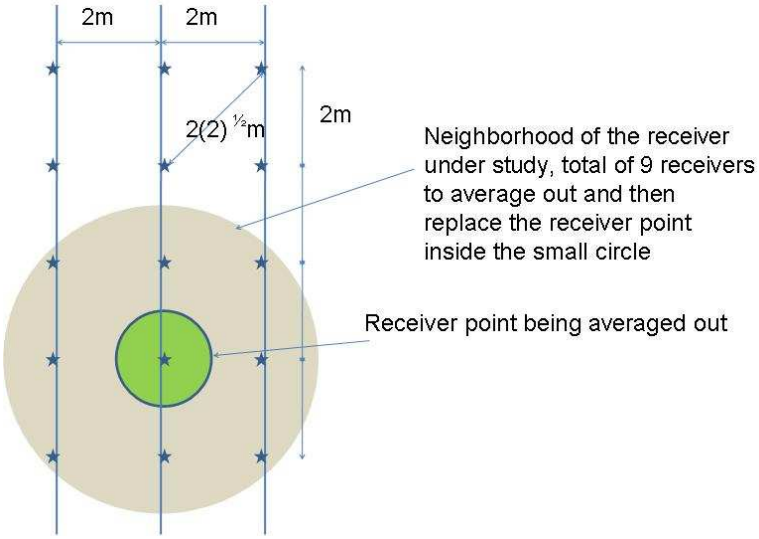

Figure 5.7. Averaging of the received power

model discussed in the previous chapter. In the L_p-norm equation given in (5.14), $r_{\nu\nu}$ denotes the predicted autocorrelation, while $\tilde{r}_{\nu\nu}$ denotes the autocorrelation of the resulting spatial process, given in (5.9). The model parameters α_n and c_n is optimized until the L_p-norm given in (5.14) reaches a local minimum. The initial values for α_n and c_n is determined from (5.12) and (5.13) respectively. We can calculate the autocorrelation of the resulting spatial shadowing process by using these model parameters in Equation (5.9). The resulting autocorrelation of the simulated shadowing process, predicted autocorrelation and theoretical autocorrelation plots are illustrated in Figure 5.8.

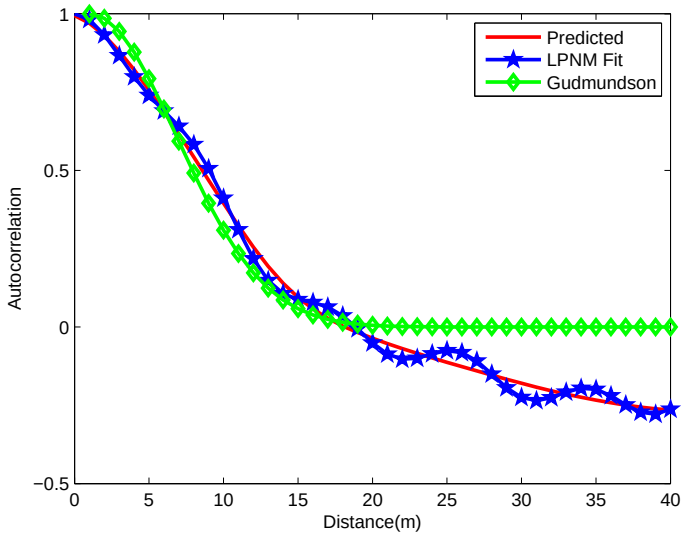

Figure 5.8. Predicted, Simulated and Theoretical Autocorrelations of Shadowing

CHAPTER 6

CONCLUSION

A low-complexity high performance Rayleigh fading simulator has been proposed. Our proposed ARMA(3,3) model has been compared with improved Jakes' model of (Zheng and Xiao 2002), AR fading filter approximation of (Baddour and Beaulieu 2005), and to the IDFT technique of (Young and Beaulieu 2000), in terms of performance measures and computational complexity. Our ARMA(3,3) Rayleigh fading generator, outperforms AR(20) generator, by about 1dB in both performance measures provided, while requiring approximately a quarter of the multiplications required by the AR(20) generator. Similarly, our ARMA(3,3) fading generator outperforms modified Jakes' generator with 8 and 16 sinusoids by 32dB and 2dB respectively, while requiring less than one-tenth of the multiplications required by the Jakes' generators with 8 and 16 sinusoids. While the IDFT method of achieves the best performance in terms of the quality measures, it brings a significant cost in storage requirements as all samples are generated using a single IFFT. Thus the IDFT method is undesirable from simulation point of view when the Rayleigh fading samples are generated as they are required. The main advantage of our ARMA(3,3) Rayleigh fading generator is that the samples of the Rayleigh fading sequence can be generated as they are required while achieving the lowest complexity of all the Rayleigh fading generators mentioned. Since multiple-input multiple-output (MIMO) antenna systems have the ability to increase capacity and reliability of a wireless communication system compared to single-input single-output (SISO) systems; for the future work, MIMO extension of our ARMA(3,3) fading generator can be developed.

We also apply the fixed-point extension of our proposed filter design. Accurate results can be obtained by using 16-bits quantized filter coefficients. But 10-bits and 14-bits quantized coefficients are not enough for the accuracy of the filtering.

The shadowing loss is easily predicted in a specific propagation experiment, by extracting the theoretical free-space path loss from the total loss, by using the site-specific radio propagation software called Wireless InSite.

A sum-of-sinusoids based spatial simulator proposed in (Pätzold and Nguyen 2004) has been used to simulate shadowing processes. Two schemes have been used

for the computation of the model parameters; the MEA and LPNM. LPNM is preferred for medium and especially for low values of the number of sinusoids. LPNM has also big advantage, because this method enables the fitting of the statistical properties of the simulator to real-world channels simply by using measured autocorrelation in order to spatial autocorrelation of the theoretical reference model. We use our predicted autocorrelation in an urban area, to fit the simulator.

Altough LPNM is a very useful method, MEA results in a closed form solution whereas the LPNM does not. When using the MEA, it can be shown that the simulation model converges to the reference model if the number of sinusoids tends to infinity.

However it has been shown that by applying the sum-of-sinusoids based simulation method on shadowing channels, the simulation model has nearly the same statistics as the reference model.

REFERENCES

Aguiar, A. and James Gross. 2003. Wireless Channel Models. TKN Technical Report TKN-03-007, Technical University Berlin.

Baddour, K. E. and N. C. Beaulieu. 2005. Autoregressive modeling for fading channel simulation. *IEEE Trans. on Wireless Commun.* 4 (4): 1650-1662.

Bello, P. A. 1963. Characterization of randomly time-variant linear channels, *IEEE Trans. Commun. Syst.* 11 (4): 360-393.

Bennett, W. R. 1948. Distribution of the sum of randomly phased components *Quart. Appl. Math.* 5: 385-393.

Black, D. M. and D. O. Reudink. 1972. Some characteristics of mobile radio propagation at 836 Mhz in the Philadelphia Area. *IEEE Trans. Veh. Tech.* 21: 45-51.

Clarke, R. H. 1968. A statistical theory of mobile-radio reception. *Bell Syst. Tech. J.* 47: 975-1000.

Cavers, James K. 2000. *Mobile Channel Characteristics* Norwell: Kluver Academic Publishers.

Fletcher, R. and M. J. D. Powell. 1963. A rapidly convergent descent method for minimization *Computer Journal* 6(2):163-168.

Giancristofaro, D. 1996. Correlation model for shadow fading in mobile radio channels. *Electron. Lett.* 32(11):958-959.

Gudmundson, M. 1991. Correlation model for shadow fading in mobile radio systems. *Electron. Lett.* 27(23):2145-2146.

Ibrahim, M. F. and J. D. Parsons. 1983. Signal strength predictions in built-up areas *Proc. IEE* 130(5):377-384.

Jakes, W. C. 1974. *Microwave Mobile Communications*. New York: Wiley.

Kim, H. and Y. Han. 2002. Enhanced correlation shadowing generation in channel simulation. *IEEE Commun. Lett.* 6(7):279-281.

Mandayam, N. B., P. C. Chen, and J. M. Holtzman. 1996. Minimum duration outage for cellular systems: a level crossing analysis. *Proc. IEEE Veh. Technol. Conf.* 2:879-883.

Marsan, M. and G. Hess. 1990. Shadow variability in an urban land mobile environment. *IEEE Electron. Lett.* 26:646-648.

Okumura, Y., E. Ohmori, and T. Kawano, eds. 1968. Field strength and its variability in VHF and UHF land mobile radio services. *Rev. Elec. Commun. Lab.* 16:825-873.

Omidi, M. J., S. Pasupathy and P. G. Gulak. 1999. Joint Data and Channel Estimation for Rayleigh Fading Channels. *Wireless Personal Communications* 10:319-339.

Özen, S. and M. D. Zoltowski. 2001. A Fading Filter Approximation to Enable State-Space Modeling and Joint Data/Channel Estimation of (Time-varying) Frequency Selective Channels with Antenna Arrays. *IEEE Circuits and Systems Society Notre Dame Workshop on Wireless Comm. and Networking*. South Bend IN.

Pätzold, M., U. Killat and F. Laue. 1996. A deterministic digital simulation model for Suzuki processes with application to a shadowed Rayleigh land mobile radio channel. *IEEE Trans. Veh. Tech.* 45(2):318-331

Pätzold, M., U. Killat and F. Laue, eds. 1998. On the statistical properties of deterministic simulation models for mobile fading channels. *IEEE Trans. Veh. Tech.* 47(1):254-269.

Pätzold, M. 2003. On the stationary and ergodicity of fading channel simulators basing on Rice's sum-of-sinusoids. *Proc. 14th IEEE Int. Symp. on Personal, Indoor and Mobile Radio Communications, IEEE PIMRC 2003*. Beijing, China.

Pätzold, M. and V. D. Nguyen. 2004. A spatial simulation model for shadow fading processes in mobile radio channels. *Proc. 15th IEEE Int. Symp. on Personal, Indoor and Mobile Radio Communications, IEEE PIMRC 2004*. Barcelona, Spain.

Perahia, E. and D. C. Cox. 2001. Shadow fading correlation between uplink and downlink. *VTC 2001-Spring*:308-312.

Pollini, G. P. 1996. Trends in handover design. *IEEE Commun. Magazine* 34(3):82-90.

Proakis, J. G. 2001. *Digital Communications*. Singapore: McGraw-Hill International.

Proakis, J. G. and D. K. Manolakis. 2007. *Digital Signal Processing: Principles, Algorithms and Applications*. New Jersey: Prentice Hall.

Rappaport, T. S. 1999. *Wireless Communications*. New Jersey: Prentice Hall.

Reudink, D. O. 1972. Comparison of radio transmission at X-band frequencies in suburban and urban areas. *IEEE Trans. Ant. Prop.* 20: 470-473.

Saunders, Simon R. 1999. *Antennas and Propagation for Wireless Communication Systems* New York: John Wiley and Sons, Inc.

Smith, J. I. 1975. A computer generated multipath fading simulation for mobile radio. *IEEE Trans. on Veh. Technol.* 24: 39-40.

Stark, H. and J.W. Woods. 2002. *Probability and Random Processes with Applications to Signal Processing*. New Jersey: Prentice Hall.

Steele, R. 1992. *Mobile Radio Communications*. London: Pentech Press.

Stüber, G. L. 2001. *Principles of Mobile Communications*. Boston: Kluwer Academic Publishers.

Xiao, C. and Zheng Y.R. 2002. A statistical simulation model for mobile radio fading channels. *Proc. IEEE Wireless Commun. and Networking Conf.* (1): 144-149.

Young, D. J. and N. C. Beaulieu. 2000. The generation of correlated Rayleigh random variates by inverse discrete Fourier transform. *IEEE Trans. on Commun.* 48(7): 1114-1127.

Young, D. J. and N. C. Beaulieu. 2001. Limitations of sum-of-sinusoids fading channel simulators. *IEEE Trans. on Commun.*, 49(4): 699-708.

Young, D. J. and N. C. Beaulieu. 2003. Power margin quality measures for correlated random variates derived from the normal distribution. *IEEE Trans. Inf. Theory* 49(1): 241-252.

Zhang, N. and J. M. Holtzman. 1996. Analysis of handoff algorithms using both absolute and relative measurements. *IEEE Trans. Veh. Tech.* 45(1): 174-179.

Zhang, W. 2000. Fast Two-Dimensional Diffraction Modeling for Site Specific Propagation Prediction in Urban Microcellular Environments. *IEEE Trans. Veh. Tech.* 49(2): 428-436.

Zheng, Y.R. and C. Xiao. 2002. Improved models for the generation of multiple uncorrelated Rayleigh fading waveforms. *IEEE Commun. Lett.* 6(6): 256-258.

Zheng, Y.R. and C. Xiao. 2003. Simulation models with correct statistical properties for Rayleigh fading channels. *IEEE Trans. Commun.* 51(6): 920-928.

Zheng, Y.R., C. Xiao and N. C. Beaulieu. 2003. Statistical simulation models for Rayleigh and Rician fading. *Proc. IEEE Int'l Commun. Conf.* 65(6): 3524-3529.